OPTIMIZING INSPECTION OF HIGH ASPECT RATIO MICROSTRUCTURES USING A PROGRAMMABLE OPTICAL MICROSCOPE

A Thesis
Presented to
The Academic Faculty

by

Joseph Thomas Ceremuga II

In Partial Fulfillment
Of the Requirements for the Degree
Master of Science in Mechanical Engineering

Georgia Institute of Technology

November, 2003

OPTIMIZED INSPECTION OF HIGH ASPECT RATIO MICTROSTRUCTURES USING A PROGRAMMABLE OPTICAL MICROSCOPE

Approved

Dr. Thomas R. Kurfess, Chairman

Dr. William P. King

Dr. Kok-Meng Lee

Date Approved: 14 Nov 2003

ACKNOWLEDGEMENT

Above all, I would like to thank my parents, sister, and grandmother for their love, support and understanding. They made me realize that hard work and determination will pay off despite any adversity encountered along the way. Special thanks to Uncle Norm for inspiration and encouragement in mechanical engineering

I would like to thank my advisor, Prof. Thomas R. Kurfess, for his support throughout this thesis research. His guidance has molded me to become a better thinker and engineer. Thanks to my thesis committee, Prof. Kok-Meng Lee and Prof. William P. King, for freely sharing their knowledge, time, and educated comments.

The project sponsor, Sandia National Laboratories (SNL) in Livermore, CA, deserves credit for the success of this project. Sandia is a multiprogram laboratory operated by Sandia Corporation, a Lockheed Martin Company, for the United States Department of Energy under contract DE-AC04-94-AL85000. Sandia has supported this research from the beginning, providing the needed metrology tools, specimens, and software development environment. To start, thanks to my Director, Jill Hruby, Deputy Director, Glenn Kubiak, and Manager, Craig C. Henderson for providing me with knowledge, opportunities, and responsibilities at Sandia as well as showing the importance of LIGA's role in microsystem technology. Thanks to my mentor, Georg Aigeldinger, and fellow colleagues, Franz Josef Pantenburg and Stanley Mrowka, for their knowledge of the LIGA process, metrology techniques, and welcomed criticism.

To my fellow officemates in 213 and friends at Georgia Tech, thank you.

TABLE OF CONTENTS

LIST OF TABLES

LIST OF FIGURES

LIST OF SYMBOLS

PMMA	Polymethylmethacrylate
SU8	Trade Name for a Negative Photoresist
mm	Millimeter
μm	Micrometer
nm	Nanometer
CMM	Coordinate Measurement Machine
AFM	Atomic Force Microscope
SEM	Scanning Electron Microscope
MCS	Machine Coordinate System
PCS	Part Coordinate System
VMS	VIEW Measurement Software
GUI	Graphical User Interface
NIST	National Institute of Standards and Technology
ISO	International Organization of Standardization
GUM	Guide to the Expression of Uncertainty in Measurement
FOV	Field of View

SUMMARY

In LIGA, as with any manufacturing process comes the need for a solid foundation of metrology so that product quality and process control may be regulated and improved upon. This work aims at both the improvement and proper understanding of data acquisition techniques for LIGA materials using a programmable optical microscope as well as the data post-processing for LIGA part delivery and process improvement.

LIGA presents high aspect ratio structures made of various materials. Free-standing metallic structures and transparent structures bonded to highly radiant metallized surfaces are examined dimensionally by means of edge detection through image processing. The lighting environment plays an integral role in the correctness of a measurement. The effects that different lighting types and intensities have on a measurement are examined for all materials native to the LIGA process. Specimens were measured using the three means of illumination offered by the microscope: coaxial, LED ring, and back lighting. Each lighting type was examined and the optimum was determined for each type of LIGA specimen. Released metallic parts are to be inspected by using back lighting similar to chrome reticle inspection. Photoresist structures are to be inspected with the coaxial light with special precautions that take edge uncertainty into consideration while improving the efficiency and reliability of the inspection. Uncertainties examined within the inspection process include the optics, the stage, temperature of the metrology lab, thermal expansion of the LIGA materials, repeatability of the microscope, and the effects of intensity changes on the measurement when comparing data sets. Once the specimen

is inspected, whether metallic or photoresist, the overall uncertainty of the measurement may be assessed for each inspection scenario.

Once the result for the overall uncertainty of the data has been obtained, the data gained from the inspection can be analyzed with confidence for metrology reports and process improvement strategies. Various software toolboxes have been developed to compliment commercially available comparator software, serving as an efficient vehicle to analyze the direct measurements taken by the microscope as well as the XYZ point cloud generated from the edges detected. The software performs real-time data overlays and statistics in the form of basic XY plots, error bar plots, histograms, and quantile-quantile plots. These software packages were created to analyze metrology data and uncover trends per feature, per part, across whole wafers, and across all LIGA process steps in an effort quantify and improve upon anomalies of the LIGA process. With these tools at hand, metrology can add quality and process control to rapid prototyping that is unique in this field [Aigeldinger, et al. 2003].

CHAPTER 1 : INTRODUCTION

Metrology plays an invaluable role in any manufacturing process. The metrology process is most basically described through data acquisition and data analysis [Choi 1996]. Data acquisition refers to the hardware, or tools selected to inspect the specimens/process at hand, whereas data analysis would involve the software that digests the data, providing meaningful output. Both of the aforementioned areas will be discussed and improved upon for the sake of advancing metrology capabilities for mesoscale (>100 μm) LIGA fabricated parts with microscale (100nm to 100μm) features [Dow and Scattergood 2003]. Using multiple lithographic steps and deep X-ray exposure, LIGA can produce high aspect ratio microstructures. A detailed discussion on the LIGA process and its abilities to fabricate microparts is given in chapter two.

Working at these scales, inspection tool selection becomes critical. While present metrology tools range from coordinate measurement machines (CMM) for cm/mm scale to atomic force microscopes (AFM) for atomic ($\mathring{A}$) scale, with other systems in between, each has its advantages and shortcomings. However, forming a system of checks and balances through the use of multiple inspection tools, in order to understand the accuracy and uncertainty of the metrology process, is welcomed.

In between the component measurement range of the CMM and that of the AFM is the optical microscope [Hibbard and Bono 2003]. With its 2D high resolution measuring capabilities, non-contact inspection, and potential for automation, this device is well suited for the inspection of high aspect ratio microstructures created by LIGA

lithography. However, by the nature of this metrology tool and high aspect ratio structures, many questions come up with regards to how the measurements are taken.

1.1 Problem Description

A programmable optical microscope suits the needs for LIGA metrology because of its speed, ability to take direct measurements, to output coordinate data, and automation potential for large numbers of samples. However, due to the nature of LIGA, many obstacles must be overcome and questions of uncertainty should be answered so that the measurements taken by this tool are understood as best as possible. Typical calibration standards for optical microscopes are made of thin (~0.1 μm) chrome patterned onto flat, glass plates. Intrinsically, this is a two-dimensional artifact with very sharp edges, minimal roughness, and virtually no topology. LIGA structures, on the other hand, have high aspect ratios (typically on the order of 10:1 feature height to width) and surfaces created by processes such as lapping, polishing, and electrochemical nucleation. The edges of these structures do not present the sharpness of two orthogonal planes intersecting each other. Instead, there is typically a "rounded" edge that is seen during inspection. Also, lighting conditions play a large role in the ability for a microscope to detect such an edge. Manufacturer's instructions for setting lighting conditions typically have guided the user to use low levels of light [VIEW Engineering 2003]. Using light sparingly avoids flooding the sensor so that image saturation or blooming does not occur. Blooming refers to a glare picked up by the sensor when an object reflects too much

light. The effects that changes in light intensity have on the edge detection need to be addressed, they are critical in assessing the uncertainty of the measurements.

Furthermore, as with any metrology process, post-processing data should be performed with consistency and output suitable for comparisons, statistics, and recognizing areas in the manufacturing process needing improvement. With LIGA still being a niche technology, guidelines regarding how the process should be qualified from a manufacturing standpoint are in their infancy [Dear03].

1.2 Objectives

The programmable optical microscope can measure features on LIGA structures with the speed, repeatability, and accuracy desired for most design requirements. The sub-micron resolution and accuracy of the microscope suits typical LIGA lateral tolerance requirements on the 1-5μm scale. Therefore, from the data acquisition perspective, an understanding of the uncertainty involved in properly inspecting LIGA parts with this type of microscope is the goal of this research. The capabilities of the microscope will be properly quantified using a certified standard for the optics with each available objective (10x, 20x, and 50x). The stage accuracy and repeatability will be tested to understand the uncertainty for measurements taken outside the field of view of the camera. Any distortions with respect to the position of the feature within the field of view will be tested and addressed. Then, the effects that changes in the lighting intensity and lighting type have on the measurement will be studied and compared for chrome standards as well as specimens with aspect ratios and materials native to LIGA. To support the

measurements taken for photoresists by the optical microscope and to examine the topology at hand, specimens will be inspected using a scanning electron microscope (SEM). Another test specimen representing the transparent photoresist materials involved in the mask-making and mold steps will be examined equivalently.

Once an understanding for the uncertainty of the acquired data is reached, the data processing side will bring forth a scheme that properly qualifies LIGA structures. By combining in-house and commercially available software packages, an efficient post-processing method will be presented and proven to display traits inherent of the LIGA process. This data processing strategy allows for the manipulation of both the direct measurements and raw edge detection point clouds to analyze measurements on scales across part features, complete parts, full wafers, and all manufacturing steps of the LIGA process.

CHAPTER 2 : BACKGROUND

2.1 Overview

As a manufacturing process grows, often times there are design changes and process parameter adjustments. These changes are generally based on data that has accumulated from monitoring the entire process chain. Dimensional metrology is often used in-line with the manufacturing process to regulate part and process quality. Therefore, in order to properly evaluate a manufacturing process, the metrology process, that which provides the inspection data, must meet well-defined requirements and be continuously scrutinized. Ultimately, if a process is not monitored or measured, it cannot be managed or controlled [ICE 1998].

LIGA, the manufacturing process under inspection in this research, is quite complex. There are many steps in this process that influence the outcome of the final part. Hence, a rigorous metrology process is an assured requirement.

2.2 Metrology

Metrology, also known as Measurement Science, was first formally recognized as an integral part of manufacturing during the 1950's [Hoskins 1969]. Motivation for an increase in dimensional calibration and certification of standards was derived from the ability to fabricate products with increasing precision [Harris 1969]. As manufacturing processes are able to fabricate smaller structures and devices with great precision,

metrology data acquisition transitions from tools such as calipers and coordinate measurement machines to the non-contact realm of optical and electron microscopy.

The integrated circuit industry has first brought about the need for metrology on a micro- and nano-scale. For the most part, linewidth structures in the semiconductor industry must fulfill design requirements based upon their electrical and thermal characteristics. These requirements loosen the geometrical tolerances with respect to feature size needed to pass inspection. For instance, the company Motorola accepts linewidth structures of +/-10% of their nominal target [Waldo 2001].

Within the field of view of a microscope or SEM, +/-10% is not a challenging design requirement for a mesoscale LIGA part. The microelectronic parts are subjected to performance testing procedures prior to acceptance to ensure proper characteristics. These testing procedures are not always an option for LIGA parts. For microstructures that must conform to lower design tolerances, special care must be taken because the required measurement accuracy is approaching the uncertainty of the optics and stage uncertainty of the inspection tools. Typically, a ratio of design tolerance to inspection uncertainty of 10:1 is desired and a minimum test accuracy ratio of 4:1 is required [Davis, et al. 2001]. For example, if there is a +/-10μm tolerance on a 100μm linewidth, an inspection process with +/-1μm of uncertainty suits the inspection.

2.2.1 Uncertainty

According to The National Institute of Standards and Technology (NIST), "A measurement result is complete only when accompanied by a quantitative statement of its uncertainty. The uncertainty is required in order to decide if the result is adequate for its intended purpose and to ascertain if it is consistent with other similar results." Uncertainty is defined by The International Organization of Standardization (ISO) as a parameter, associated with the result of a measurement, which characterizes the dispersion of the values that could reasonably be attributed to the measurand. Many questions regarding uncertainty can be answered by consulting *The Guide to Expressing Uncertainty in Measurement* (GUM). GUM was published by a metrology group, created by ISO, in order to set "general rules for evaluating and expressing uncertainty in measurement that can be followed at various levels of accuracy and in many fields – from shop floor to fundamental research." [NIST 1994]

Uncertainty, for a measured value Y, may originate from N number of quantities X during a measurement (Equation 2.1).

$$Y = f(X_1, X_2, ..., X_N) \tag{2.1}$$

Along with each value for X_i contributing to the measurement Y come correction factors that take variables such as different environment conditions, observers, and instruments, etc. This ensures that the value expressed contains information based on theory as well as its measurement process.

A standard uncertainty, u_i, is the most common means of representing uncertainty. This is done by calculating the positive square root of the estimated variance u_i^2, or more widely known as taking the standard deviation, s_i.

When dealing with uncertainty, there are two common situations, Type A and Type B. Type A deals with evaluating the sample mean (Equation 2.2) and standard deviation (Equation 2.3) of a series of independent observations. This is a statistical method for working with data.

$$x_i = \overline{X}_i = \frac{1}{n}\sum_{k=1}^{n} X_{i,k} \tag{2.2}$$

$$u(x_i) = s(\overline{X}_i) = \left(\frac{1}{n(n-1)} \sum_{k=1}^{n} \left(X_{i,k} - \overline{X_i} \right)^2 \right)^{\frac{1}{2}} \tag{2.3}$$

Type B analysis of uncertainty incorporates all information known about the measurement process, not just the measured data. Examples of information included in the uncertainty are previous measurement data, general knowledge of the behavior of the testing/measuring apparatus and environment, claims of the manufacturer with respect to materials and instrumentation, calibration data, and uncertainties attributed to reference data taken from manuals. Once the uncertainty is accounted for, the data must be modeled after a chosen distribution. Common choices are a uniform (rectangular) distribution, triangular distribution, and the most widely used, the normal (Gaussian) distribution. A rectangular distribution is used when the probability of an occurrence is

the same for all sampled values [Weisstein 2003]. Triangular distributions model data from a subjective analysis where little information is known; such as only the maximum, minimum, and a guess of the modal value [Brighton 2003]. Gaussian distributions are used to describe natural and industrial processes. They are defined by a mean and standard deviation in a bell-shaped curve [Brighton 2003].

A confidence interval is then set on the data indicating a certain percentage of confidence that a random sample from the population will fall within the upper (a_+) and lower (a_-) limits defined by this interval. For instance, when assuming a normal distribution, common values of confidence used throughout manufacturing processes are 67%, 95%, and 99.73%, corresponding to coverage factors (k) of one, two, and three standard deviations from the mean when assuming a normal distribution. The value obtained by multiplying the uncertainty by a coverage factor is called the expanded uncertainty. When a process has more than one source of uncertainty, the combined standard uncertainty must be calculated. A very conservative method for calculating combined uncertainty, $u_c(y)$ would be to sum the absolute values of the uncertainties. However, NIST suggests using a different approach. For an uncertainty $u(x_i)$ multiplied by some constant a_i, such as a coverage factor, for N sources of uncertainty, combined standard uncertainty is calculated using Equation 2.5 below [NIST 2003].

$$u_c^2(y) = a_1^2 u^2(x_1) + a_2^2 u^2(x_2) + \ldots + a_N^2 u^2(x_N) \tag{2.2}$$

Uncertainty, in the case of metrology, refers to the extent that an inspection process may be considered accurate. Although a single, finite quantity is desired in measuring an

artifact, in essence, it is unattainable without assessing some degree of error. Thus, pertinent measurements (Y) in this report will be accompanied with an uncertainty based upon a stated approximation of confidence as shown in Equation 2.6.

$$Y = y \pm u_c(y) \tag{2.3}$$

This report follows a Type B evaluation since it examines the uncertainty of the measurement setup as well as the uncertainty within the gathered data. The collected data will be treated under the assumption that it most closely follows a standard normal distribution.

2.2.2 Calibration

Calibration provides the user with an understanding of the uncertainty that the inspection tool contributes to the measurement. Through the inspection of standards having features certified to accredited laboratories such as NIST (US), NPL (UK), and PTB (Germany), systematic errors of instruments can be recognized and either corrected for future use or adjusted into measurements previously taken. All inspection tool hardware, such as a stylus, probe tip, optics, and staging equipment must be calibrated.

Optical microscopes are calibrated using bright chromium photoplates. This type of reticle is patterned in approximately 100nm thick chromium on glass, enough to achieve 100% opacity in visible light [Menz, et al. 2001]. The surface topology of the chromium

has an RMS roughness of about 5nm. Therefore, edges appear to be very sharp when backlit during inspection. Standards that have circular patterns of sizes where the entire feature is within the field of view of the camera, for the current magnification, are used to calibrate the optics. A length value is assigned to represent the pixel size for each lens so that measurements determined by image processing are correct.

To calibrate the XY stage positioning, chrome on glass grid plates that span the extents of the microscope stage have linewidth or circular features arranged in a rectangular array. The stage is programmed to locate these points repeatedly using an assortment of routes to see how well a point may be located and reproduced across a certain distance of travel.

Z axis calibration is performed using a step-height standard. This object has flat surfaces positioned at increasing elevations. The surfaces have an amount of roughness that is easy to focus upon. Once the image is in focus, the Z-axis height is recorded and compared to the certified value at that corresponding elevation. Figure 2.1 shows a circular chrome standard and a step-height standard.

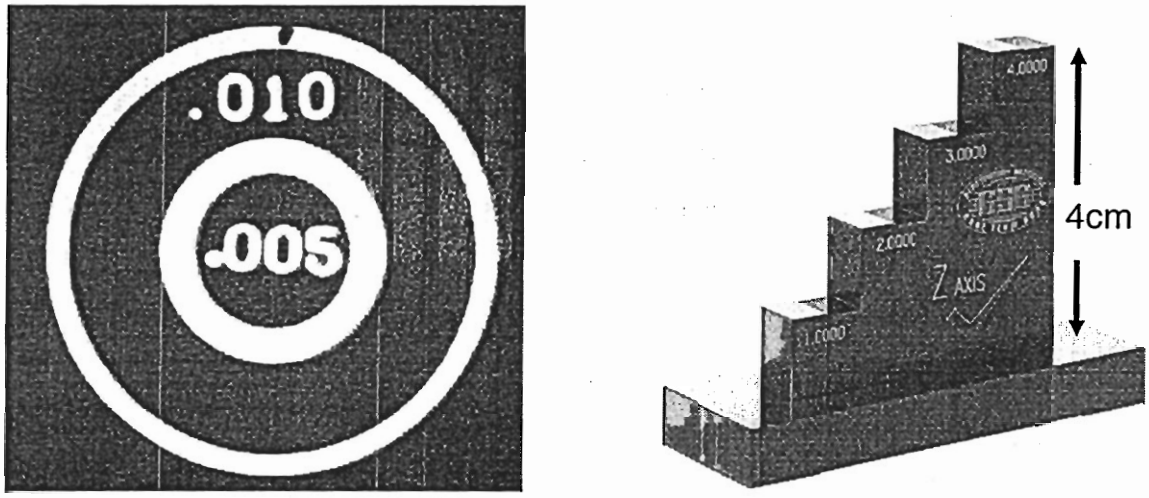

Figure 2.1: Microscope image of a chrome circular standard (left) and photograph of a step height standard (right)

Once the instrument is calibrated, measurements can be taken with confidence about traceable certifications.

2.3 The LIGA Process

The LIGA process was developed in the early nineteen-eighties at Research Center Karlsruhe, Germany, in an effort to precisely fabricate microscopic nozzles for the separation of uranium isotopes [Menz, et al. 2001]. LIGA is a German acronym for lithography (Lithographie), electrodeposition (Galvanoformung), and molding (Abformung). This process uses deep X-ray lithography to create high aspect-ratio microstructures with great accuracy.

In the beginning of a process run, an X-ray lithography mask of the design must be produced. The computer aided drawing of a design is transferred to chrome on glass UV-lithography mask using a commercial electron-beam process [Menz, et al. 2001]. To create the X-ray mask, positive or negative photoresist (e.g. Novolac or SU-8) is spun on a thin mask membrane [DOW Chemical 2003]. The mask blank is exposed and developed. The open regions are filled with gold to absorb the X-rays [Madou 1997].

At the synchrotron, which is used for the X-ray lithography step, the X-ray working mask is placed in front of a high molecular weight positive photoresist, typically polymethylmethacrylate (PMMA), which has been bonded to a substrate that has electrically conductive material characteristics (Figure 2.2).

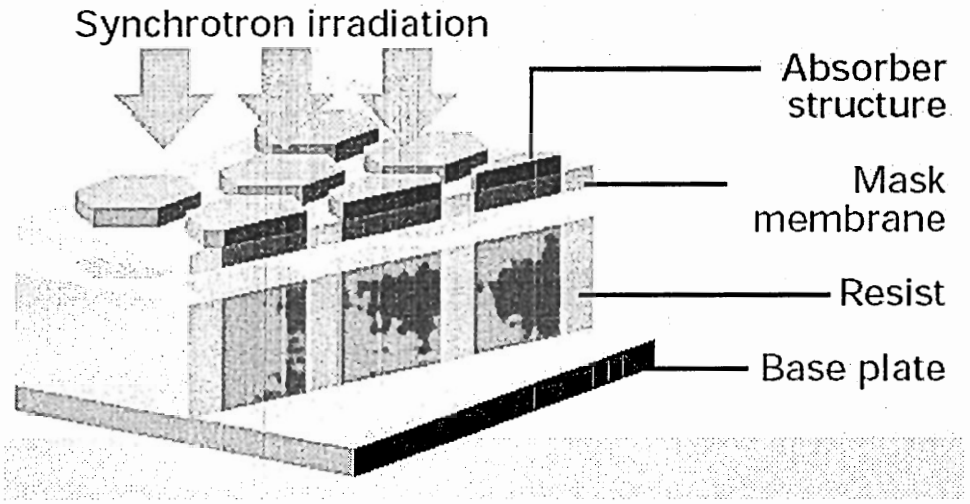

Figure 2.2: X-ray exposure of PMMA [IMM 2003]

The thickness of the PMMA resist determines the thickness of the final part, which serves as the mold in the LIGA process. During exposure, main chain scission of the PMMA polymer reduces the mean molecular weight by two orders of magnitude. Using an organic development bath, the exposed areas of the PMMA are dissolved, leaving structures with very precise sidewalls having only minor deviations from a perfect vertical (Figure 2.3) [Menz, et al. 2001]. Using a suitable X-ray mask, surface roughness characteristics of the sidewalls can be of optical quality yielding mean average roughness values of approximately 20-50nm or less [Hecht 2002]. Sidewall normality depends upon mask and beam alignment during exposure, secondary radiation effects, and the material characteristics of the mold [Menz, et al. 2001].

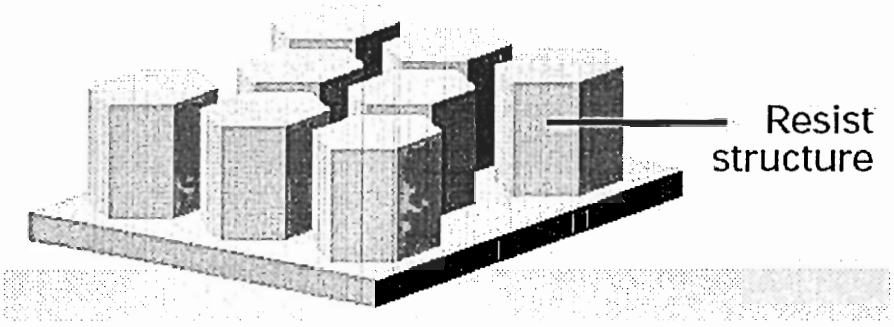

Figure 2.3: PMMA structures after development [IMM 2003]

Metal is then electroplated as a mold for future use in injection molding or as direct LIGA parts to be released from the substrate (Figure 2.4). This research deals with inspecting direct LIGA parts, made from nickel and nickel alloys.

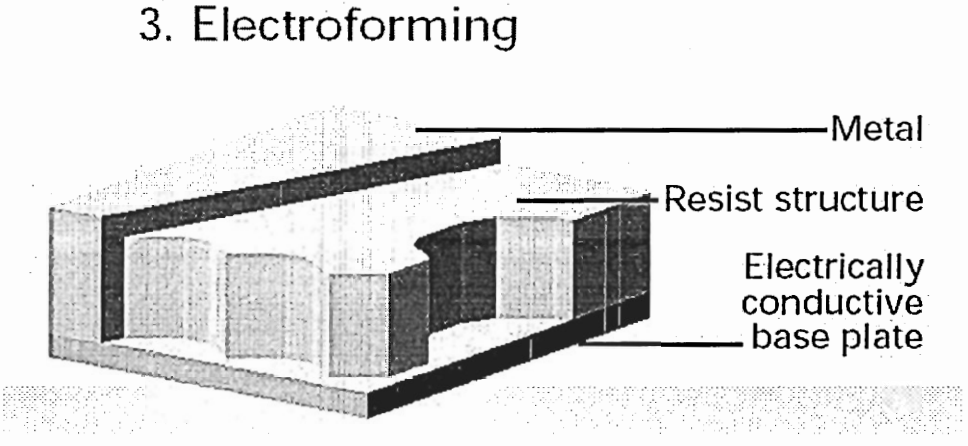

Figure 2.4: Electroplated metal around PMMA structures [IMM 2003]

To produce these released LIGA microstructures, the PMMA mold is overplated to ensure that mold is filled to the top. Lapping and polishing procedures planarize and

polish the top surface removing PMMA and the nickel overplating to part thickness specifications. The PMMA resist is then stripped from the substrate leaving only the bare electroplated parts to be released. The parts are chemically released by dissolving a thin copper layer, which was electroplated into the mold, between the parts and the substrate without damaging the microparts.

LIGA has been considered a technology that bridges the qualities of silicon microfabrication and classical high precision machining. This technology provides an elegant solution for creating two-and-a-half dimensional (two-dimensional with a thickness) meso- and micro-scale structures with unprecedented aspect ratios and absolute tolerances [Madou 1997]. The ability to use the structures as a mold for casting, offers much potential for commercial applications for having faster reproduction times than the lithography step [Menz, et al. 2001]. Materials available for LIGA are electrodeposited metals as well as all those used in molding processes such as plastics, ceramics, etc. To help current process control and improvement, sound metrology methods are in demand.

CHAPTER 3 : DATA ACQUISITION HARDWARE

To suit the needs of LIGA metrology from a manufacturing and process development standpoint, inspection tools must exhibit high resolution, great accuracy, automated control, and the ability to acquire data at relatively high speeds. These requirements seem quite standard for any inspection process, but due to the scale and theoretical resolution at which LIGA is able to produce parts, tool selection is non-trivial. A potential situation that must be avoided is to trust the judgments made by inspection data without knowing if the uncertainty of the inspection is greater than that of the size of the manufacturing process. Once this uncertainty is addressed, then proper considerations dealing with process improvement may be made accordingly. Ranges of meso-scale metrology tools are summarized in the graph in Figure 3.1 below.

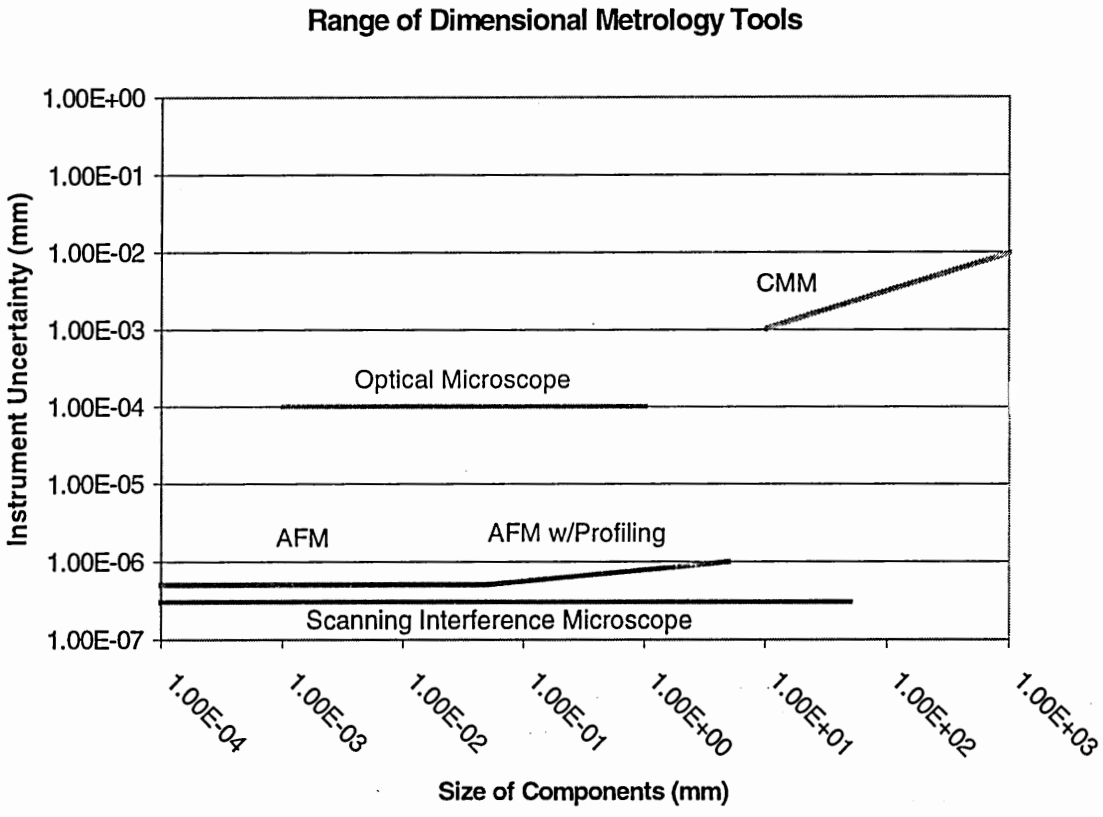

Figure 3.1: Metrology tool uncertainty and application ranges [Hibbard and Bono 2003]

By the nature of the traditional LIGA lithography process, designs are limited to two dimensions and a thickness. The dimensions of LIGA parts can be centimeters in lateral design space, millimeters in thickness (Z), have features on the order of tens of microns, and require inspection to micron precision. There are many aspects of a LIGA micropart that need to be inspected, so it is necessary to chose the most effective tool for the task. Below is a schematic of a representative LIGA structure with labeled areas of interest for metrology (Figure 3.2).

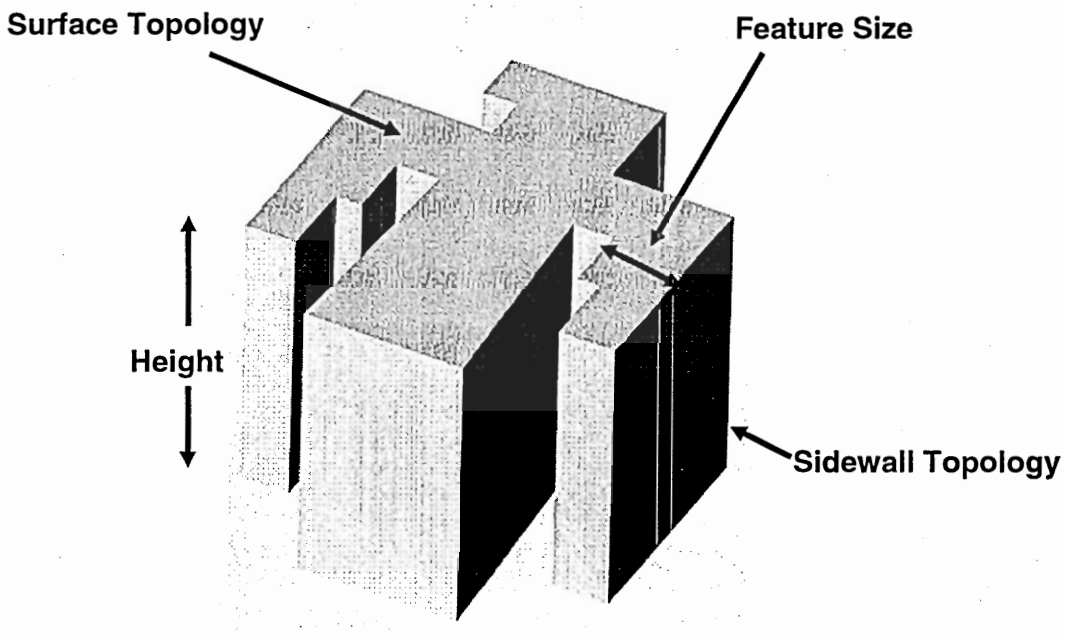

Figure 3.2: Characteristic LIGA structure and inspection points

Inspecting surface topology and sidewall quality is done most efficiently by using either a stylus profilometer or an interferometer. Feature size measurements, on the other hand, could be done by various means. Regarding accuracy and highest resolution, as shown in the above figure (Figure 3.2), one would use an AFM and/or an SEM. However, due to mass production and numerous critical features per part under inspection, these options are not feasible when considering the time required to inspect each part. Throughput is the main reason for using a programmable optical microscope for LIGA dimensional metrology. Also, regarding part size, a one centimeter part would require data set stitching and stage automation because of the size of the field of view when measuring a complete part via SEM or AFM.

3.1 VIEW Voyager V6x12 Optical Microscope

Optical microscopes have been used since the seventeenth century [Hecht 2002]. While optical microscopes are well established instruments, advancements along the lines of cameras, motorized high precision multiple axis stages, adjustable lighting conditions, variable lighting types, and software have extended the abilities of the basic light microscope to be a dimensional metrology tool.

VIEW Engineering manufactures the Voyager V6x12 programmable optical microscope (Figure 3.3) that has been used [VIEW Engineering 2003]. Table 3.1 shows the specifications of the manufacturer.

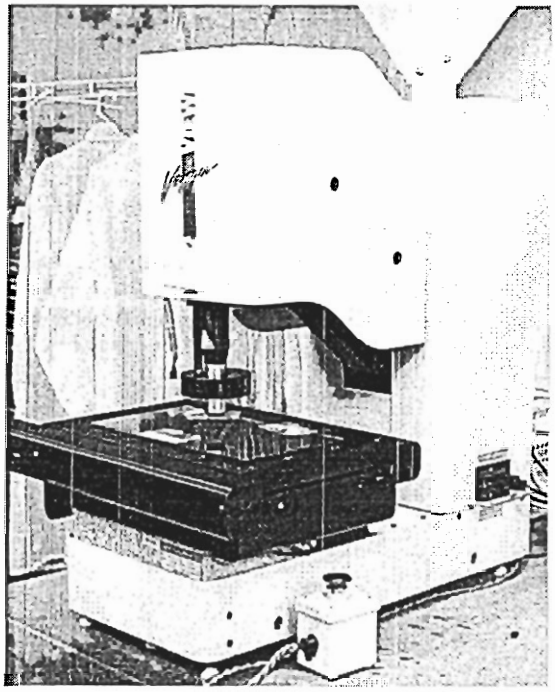

Figure 3.3: VIEW Voyager V6x12 programmable optical microscope

Table 3.1: Manufacturer specifications of the Voyager optical microscope

Instrument	VIEW Voyager V6x12 Microscope
Resolution	0.1 μm
Optical System	Single magnification fixed lens
Lighting System	Coaxial, back, and multi-colored LED
Optical Sensor	Monochrome CCD 758x581 pixel array
Image Processing	256, 8-bit, grayscale gradient processing
Stage Uncertainty (XY)	(3.5+L/300)μm*
Stage Uncertainty (Z)	(3.5+L/50)μm*

*L is measuring length in mm. Applies to a thermally stable machine and artifact @ 20° C +/- 0.5° C using a 6.6x objective lens.

The VIEW Voyager microscope is equipped with a motorized XY stage and a vision system comprised of various objectives and a monochrome charge-coupled device (CCD). The strength of this instrument is its software capability. The edge detection algorithms built into the software perform grayscale gradient image processing with contrast dependent sub-pixel interpolation. This allows the measurement accuracy to exceed the limitations of the pixel size. The software requires that the user places "finders" (Figure 3.4), with respect to either the machine coordinate system (MCS) or a user-defined part coordinate system (PCS), on the part edge undergoing inspection. The finder indicates the area where an edge is to be expected, and it gives the software an initial guess for the expected shape of an edge. Figure 3.4 shows a rectangular finder, where circular and arc finders are also available. The positions of the finders can be saved in a macro so that the inspection routine may be performed repeatedly on parts with the same geometry. This allows the user to add a large degree of automation in the data acquisition process.

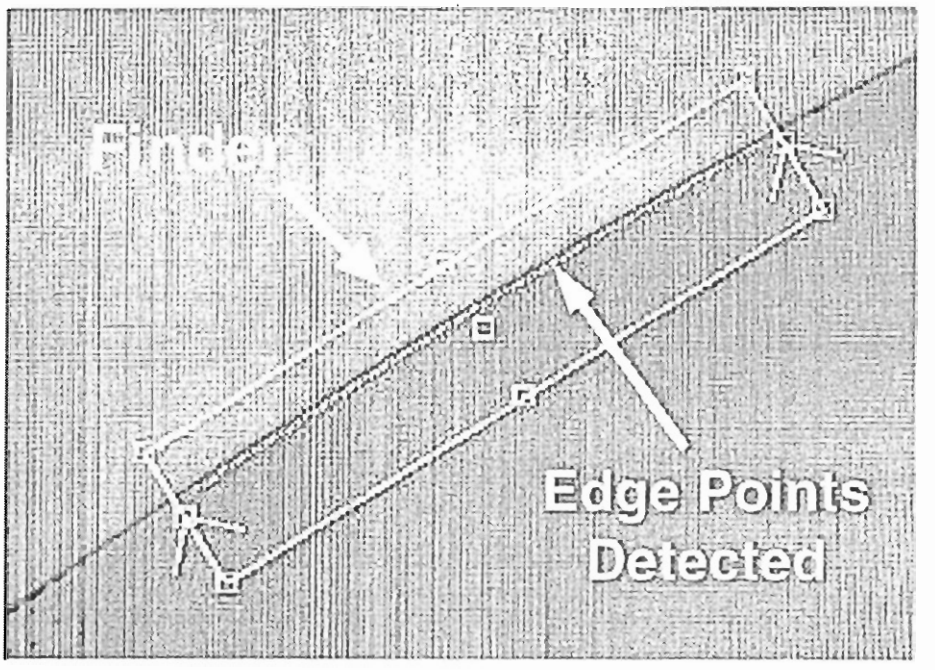

Figure 3.4: Example of a finder

The role of the Voyager is two-fold, saving both direct measurements and XYZ coordinates of the inspected edges so that further processing can be performed. Direct measurements refer to the calculations that the VIEW Measurement Software (VMS) performs, using proprietary algorithms, on various basic geometries such as lines, arcs, circles, and slots. These algorithms involve optimized fits of the basic geometries to the edge detected points.

The user has control over the environment that governs the edge detection. Lighting options include the use of a coaxial (top) light, a back light, and an LED ring light. Options such as contrast and sharpness control the edge detection algorithm once the properly lit and focused image is captured. These, as well as other parameters are used to

detect an edge when image contrast is not desirable within the boundaries of the finder [VIEW Engineering 2003].

The Voyager microscope provides the primary means for which the dimensional metrology data is acquired. The purpose of this work is to qualify and establish measurement procedures using the Voyager microscope for high throughput data acquisition. The hardware and software of this tool are commercially available, and used as supplied by the vendor. The next two sections of this chapter introduce other tools that ma be used to verify various features seen by the Voyager as well as to hone the edge detection accuracy.

3.2 WYKO NT3300 Interferometer

A white light interferometer is used to capture the topology of a specimen by using the interference signal of two beams of light generated from the same source. Once the beams are recombined, the dark and light bands, known as "fringes", compose the interferogram [Olszak, et al. 2001]. These fringes look similar to those of a topographical map, displaying the peaks and valleys of the surface scanned. Veeco Metrology Group produces the WYKO NT3300 white light interferometer that has been used in this work (Figure 3.5).

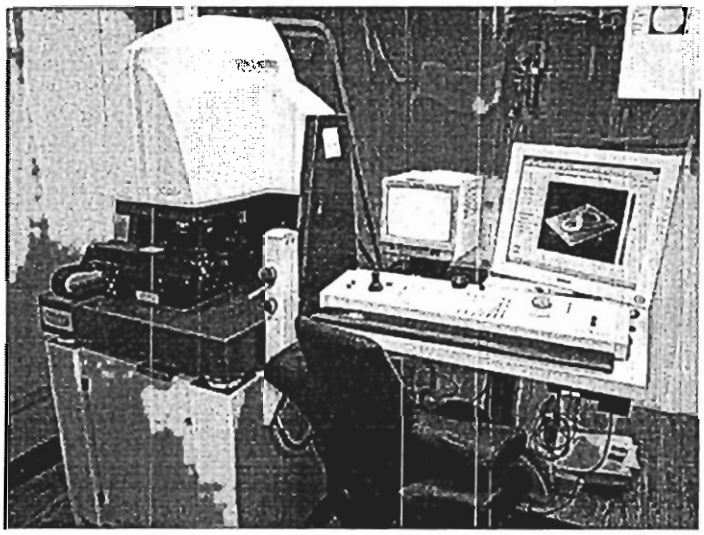

Figure 3.5: WYKO NT3300 interferometer

This device has sub-nanometer resolution in the z-direction. When considering lateral resolution at high magnifications, the resolution is also quite exceptional, as long as the edge topology is relatively flat. This is the drawback to using the interferometer for acquiring edge-to-edge feature measurements from LIGA parts. A typical LIGA part may exhibit a filleted edge attributed to various process parameters. Therefore, pertinent edge data may not be acquired due to light that is reflected away from the sensor on angled/sloped surfaces. Regardless, scanning the surface of a LIGA structure still provides valuable data in the effort to understand the characteristics of typical LIGA part edges (Figure 3.6).

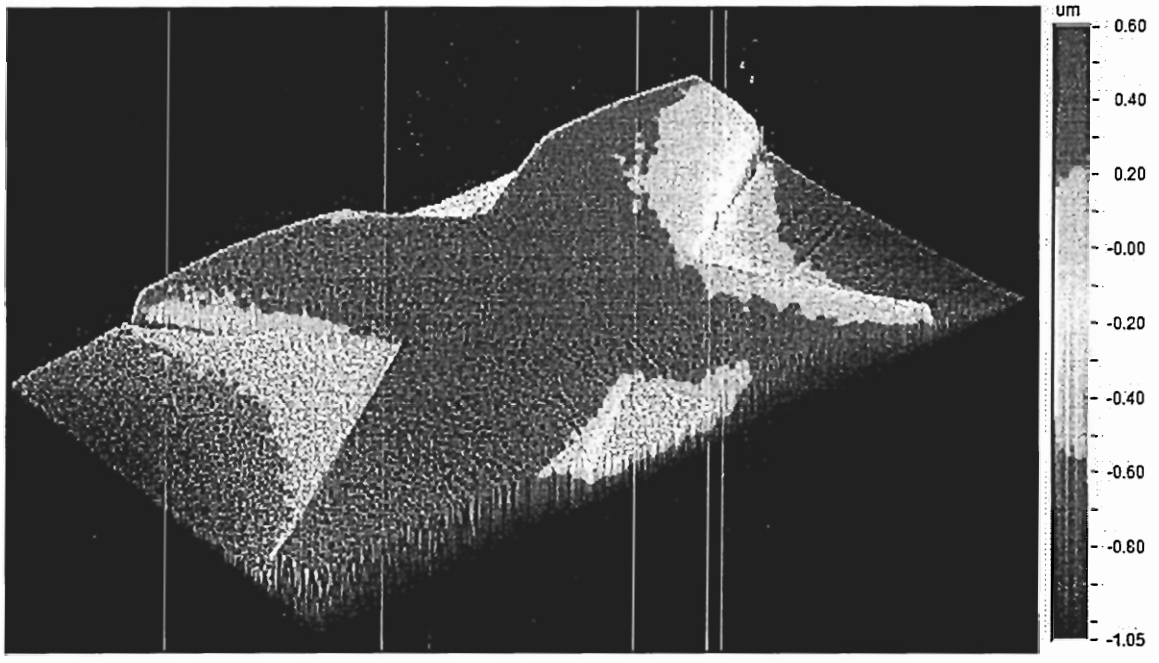

Figure 3.6: Scanned section of a metal LIGA structure embedded in PMMA photoresist using the Veeco NT3300

3.3 JEOL SEM

Next to atomic force microscopy, scanning electron microscopy exhibits extremely high resolution for measurements. An electron gun accelerates electrons through a series of lenses. The lenses reduce the beam diameter to form a small (~10nm diameter) focused electron beam on the specimen so that sharp images at high magnification can be generated. The interaction between the electron beam and the conductive specimen generates signals from secondary and backscattered electrons. An E-T (Everhart-Thornley) electron detector collects these electrons. The electrons pass through a photomultiplier tube, and their signal is then multiplied electronically and formed into an

image [Goldstein, et al. 1992]. The measurements taken with the SEM will be used to verify those taken by the Voyager optical microscope.

CHAPTER 4 : EXPERIMENTAL SETUP

Various factors, such as lab environment, the properties of materials native to LIGA, and the staging and optics of the microscope, will be examined to get an understanding for the level of uncertainty that each component contributes to a measurement.

4.1 Lab Environment

The microscope is located inside a cleanroom tent to minimize airborne particulates from settling on the microparts. Temperature data was logged every five minutes during a five-day period representing a typical workweek when the instrument would be operating. Figure 4.1 shows the results from the temperature recorder.

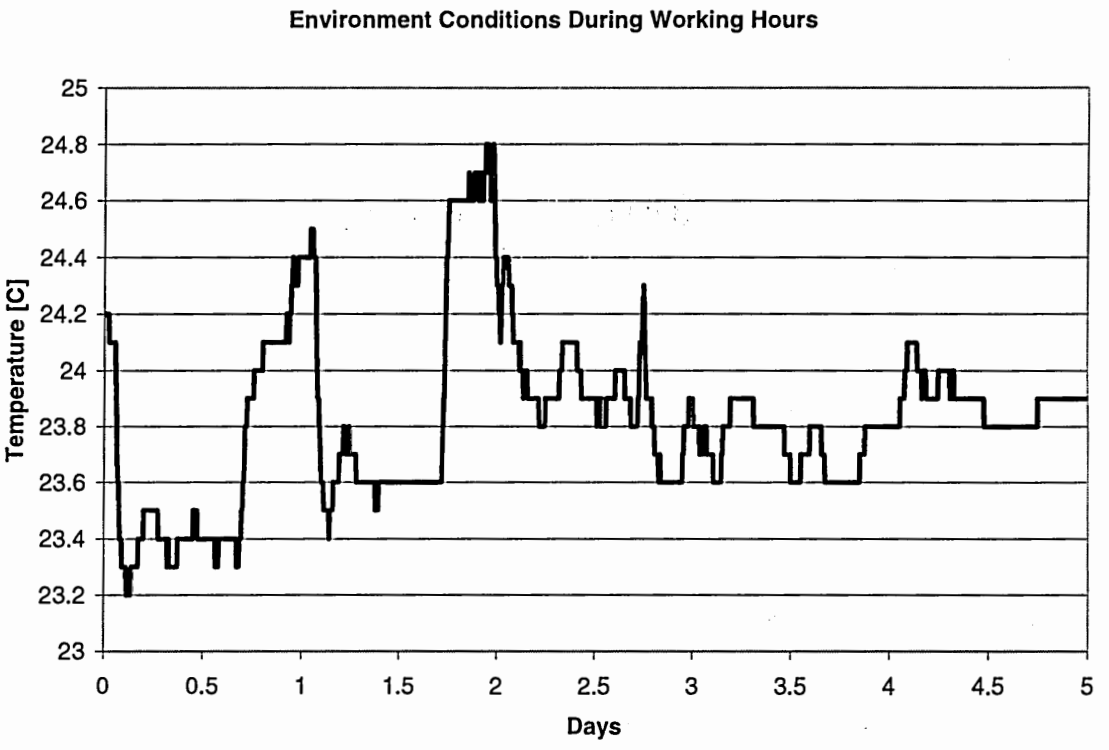

Figure 4.1: Metrology lab temperature plot

According to the data, the temperature is maintained at 23.8 degrees Celsius with a range of ± 1 degree. The temperature control in this environment is acceptable compared to standard at high resolution integrated circuit inspection facilities. These labs maintain ± 2 degree temperature control [ICE 1998]. This information is used to examine material expansion effects when comparing measurements that have been obtained at different temperatures. Table 4.1 contains the coefficients of thermal expansion for various materials native to LIGA and this study.

Table 4.1: Coefficients of thermal expansion

Material	CTE [μm/m-C]
Aluminum	22.2
Chromium	6.2
Copper	17.7
Glass	5.9
Gold	14.2
Nickel	13.0
PMMA	70-77
Silicon	2.9
Stainless Steel	16
SU8	70-77
Titanium	8.9

For instance, a nickel microstructure may have a 150μm linewidth. Therefore a 2 °C rise in temperature would expand the line by 0.004μm. On a larger scale with a 2 °C temperature change, a one centimeter nickel part would expand 0.26μm and a four-inch silicon wafer would expand 0.59μm. These are process variables that could add to measurement uncertainty, especially on the wafer scale, if the room were not temperature controlled.

4.2 The Microscope Optics

The microscope is equipped and calibrated for low, medium, and high magnification lens at 1.6x, 3.3x, and 6.6x magnification, respectively. However, for the scale of LIGA parts, objectives with 10x, 20x, and 50x magnification lenses are used. For each

objective, the field of view is calculated with respect to the calibrated length (xy) per pixel value. According to the numerical aperture values of the objectives, an estimate of the depth of focus may also be obtained by using Equation 4.1 [Hecht 2002].

$$DOF = 0.5\frac{n\lambda}{NA^2} \tag{4.1}$$

In the above equation, n is the index of refraction of the medium, lambda is the wavelength of light, and NA is the numerical aperture of the lens. Table 4.2 shows the parameters of interest for each objective.

Table 4.2: Characteristics of the objectives

	Mitutoyo Apo 10	Mitutoyo Apo 20	Mitutoyo Apo 50
Magnification	10x	20x	50x
Calibration [µm/pixel]	1.1000	0.5521	0.2056
Field of View [µm x µm]	834 x 639	418 x 321	156 x 120
Numerical Aperture	0.28	0.42	0.55
Depth of Focus [µm]	±3.5	±1.6	±0.9

For each of these objectives, various tests were performed using certified chrome reticles so that a thorough understanding of the capabilities of the instrument was achieved.

4.2.1 Calibration of the Optics

Each objective was calibrated using a chrome circular standard, NIST traceable to ± 1μm. The circle sizes used were 254μm, 127μm, and 63.5μm, for the 10x, 20x, and 50x magnification, respectively. The chosen circle was centered in the field of view prior to measurement. The feature size was chosen so that the circle appeared large, approximately two-thirds of the field of view. A single value for the size (vertical and horizontal length) of each pixel was determined by entering the certified diameter of the circular feature and comparing it to the best fit circle calculated from the points found through image processing.

In LIGA microfabrication, the linewidth of a channel or structure is typically of interest. To understand the ability of the microscope to measure a linewidth, a NIST and NPL certified chrome pitch standard (±0.266μm) was chosen to be the first specimen to undergo testing. The reticle, a Geller MicroAnalytical Laboratory MRS-3 pitch standard, has 50μm and 500μm horizontal and vertical pitches suitable for optical microscope inspection. Measuring the pitches on this standard will reveal systematic errors in the current calibration for linewidth measurements.

For each objective, the corresponding pitch size fitting within the field of view of the camera was measured. The pitch pattern on the standard consists of four quadrants: top, bottom, left, and right. Each quadrant contains six 500μm pitches and eight 50μm pitches. Ten measurements were taken at each pitch location. For the 20x objective, measurements were taken at pitches of 50μm, 100μm, 150μm, and 200μm. Both vertical and horizontal orientations were measured. The uncertainties of the pitch standard for

these distances were calculated using the combined standard uncertainty formula (Equation 2.5) [NIST 1994]. The pitch standard measurement results are shown in Table 4.3 and Table 4.4 below.

Table 4.3: Pitch standard measurement results (Vertical orientation)

Lens	Pitch [μm]	U_{cert} [μm]	Mean Dev ± σ [μm]	Range [μm]
50x	50	0.266	0.18 ±0.08	0.25
20x	50	0.266	-0.15 ±0.08	0.26
20x	100	0.376	-0.33 ±0.09	0.28
20x	150	0.461	-0.51 ±0.05	0.17
20x	200	0.532	-0.70 ±0.11	0.39
10x	500	0.267	-0.91 ±0.14	0.43

Table 4.4: Pitch standard measurement results (Horizontal orientation)

Lens	Pitch [μm]	U_{cert} [μm]	Mean Dev ± σ [μm]	Range [μm]
50x	50	0.266	0.23 ±0.05	0.17
20x	50	0.266	-0.13 ±0.04	0.12
20x	100	0.376	-0.31 ±0.04	0.11
20x	150	0.461	-0.48 ±0.04	0.12
20x	200	0.532	-0.60 ±0.06	0.22
10x	500	0.267	-0.72 ±0.04	0.15

The results show that there is a systematic error in the pitch measurement for each objective. The repeatability (Equation 4.2) of the microscope is understood by taking an average of the standard deviations found in the measurements and using a coverage factor of two for 95% confidence.

$$U_{repeatability} = 0.14\mu m \tag{4.2}$$

The results also indicate that the microscope has the potential to inspect with greater accuracy if calibrated by a more accurate artifact since the absolute values of the systematic errors are greater than the repeatability.

These tests were performed using back lighting, not the LED ring lighting or coaxial (top) lighting, at one level of intensity which created an image of acceptable contrast for edge detection. The lighting intensity and light type is adjusted by the user to find an "acceptable" amount of contrast, and each user is different. Thus, the effects that various lighting types and intensities have on the measurement will be addressed in Section 4.4.

4.2.2 Field of View Considerations and Testing

The size of the field of view should be taken into consideration when choosing an objective. When a measurement has to be performed on a feature larger than the field of view, uncertainty of the stage must be considered in the measurement. It is most desirable to choose an objective so that a critical design feature of a specimen is largest within, but does not exceed the boundaries of the field of view. This suggestion has the potential to introduce error into the inspection. Due to the nature of optical equipment, barrel distortion, a type of monochromatic aberration (Figure 4.2), may be present in the optics as features are located away from the center of the field of view [Hech01].

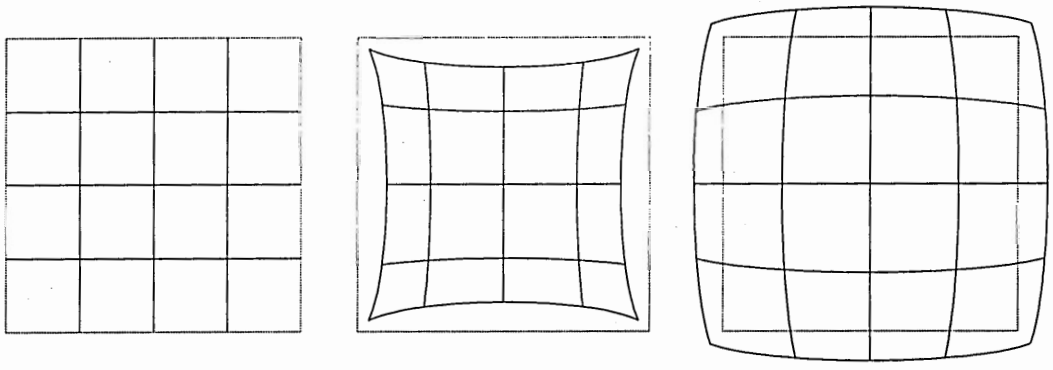

(a) (b) (c)

Figure 4.2: Undistorted image (a), negative barreling (b), and positive barreling (c)

In this case, selecting an objective would be more difficult than what was previously stated above. To understand if barrel distortions are in the Voyager's optics, a 50μm pitch from a chrome pitch standard was measured ten times, at ten different positions oriented vertically and horizontally within the field of view of each objective. Backlighting was used and left unchanged throughout the experiment for each objective once the image had an acceptable amount of contrast. The pitch measurements taken are calculated using the custom "slot" algorithm performed by the software of the microscope. A diagram of the test is shown in Figure 4.3 below. The outside border represents the field of view of the microscope.

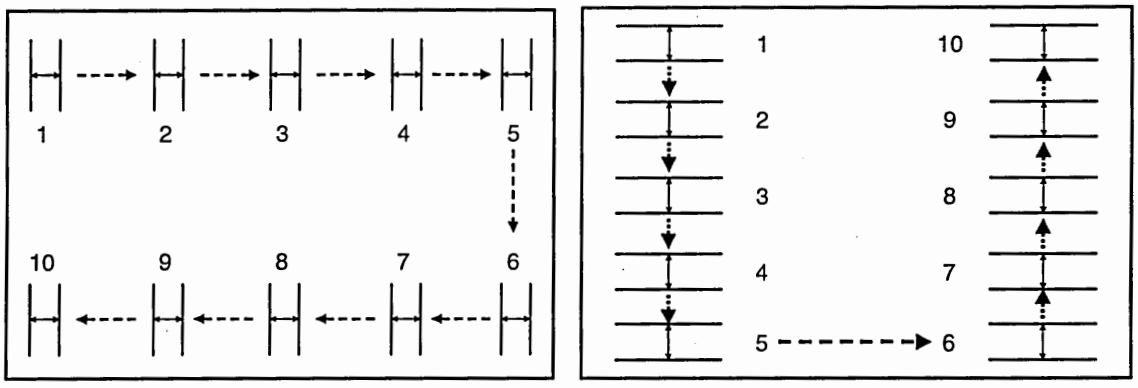

Figure 4.3: Field of view optical distortion test

Figure 4.4 below is a graph of the averages taken from the ten measurements at each of the ten positions.

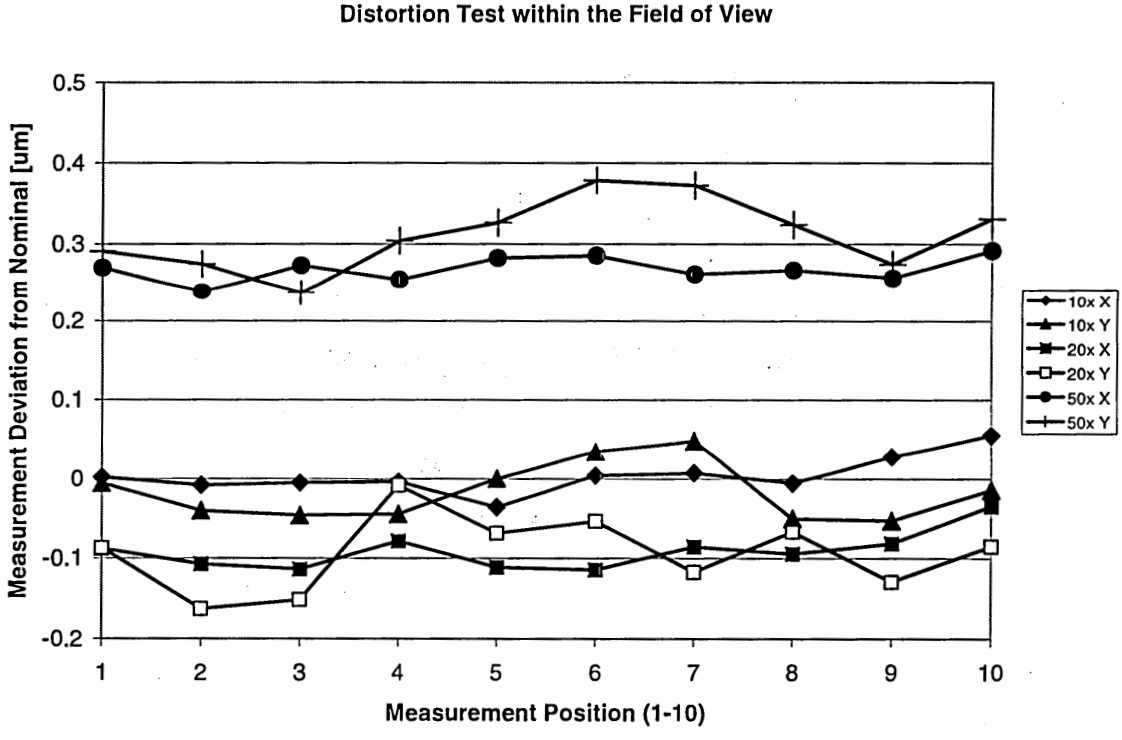

Figure 4.4: Distortion test results (10x, 20x, 50x)

No significant trends depending on XY position appear to be present in the data. Table 4.5 shows the results of the distortion test in terms of the mean and standard deviation of the measurements from the nominal 50μm pitch.

Table 4.5: Field of view distortion test results (averages)

Objective	Orientation	Mean [μm] $\pm\sigma$[μm]	Range [μm]
10x	Horizontal	0.004 $\pm$0.035	0.115
10x	Vertical	-0.017 $\pm$0.048	0.159
20x	Horizontal	-0.091 $\pm$0.033	0.098
20x	Vertical	-0.093 $\pm$0.070	0.213
50x	Horizontal	0.268 $\pm$0.053	0.162
50x	Vertical	0.311 $\pm$0.053	0.294

The standard deviation for each distortion test corresponds to those observed for the repeatability of the microscope. Therefore, no distortion is present in these lenses. Since an understanding of the accuracy and repeatability of measurements taken using only the optics has been gained, the next step is to assess the abilities of the stage for non-field of view inspection.

4.3 The Microscope Stage

The DC servo motor controlled stage cradles a glass plate allowing for a six by twelve inch measuring area. The relation in Equation 4.3 was provided by the manufacturer for the uncertainty of the stage.

$$U_{XYplane} = \left(3.5 + \frac{L}{300}\right)\mu m \tag{4.3}$$

Stage accuracy and repeatability is determined once a year by a VIEW Engineering technician. The tests are performed using a high accuracy 150x300mm chrome grid plate with features NIST traceable to $\pm 1.95\mu m$. Features 10mm apart in a 16x31 rectangular array are inspected. The XY test inspects each point on the grid five times. VIEW compiles the data by taking the mean and standard deviation of the five measurements. A coverage factor of three (99.73% confidence across a standard normal distribution) is used on the standard deviation. The values considered were the maxima of the means, the standard deviations, and the ranges across the XY locations.

To verify the stage repeatability and accuracy more frequently, position repeatability tests are performed using an in-house available certified six by nine inch chrome-on-glass grid plate by Vidicomp (Figure 4.5). The reticle, a three by three rectangular array of circular chrome features has been certified to NIST traceability by Sandia National Laboratories Manufacturing Processes and Services Department, to $\pm 1.54\mu m$ in XY position and feature size. The inspection program implemented specifically for this task aligns the microscope in the x-axis based on a line constructed from the centers of circles #4 and #6. The y-axis is created from a line normal to the x-axis, passing through the

center of circle #5. This repeatability test is performed to show the ability of the microscope to reproduce the XY coordinates of the center of circle #5 as the stage traveled in four different patterns. The four different patterns were chosen so that the stage approached circle #5 from each of the corners. Figure 4.5 shows the travel in one of the four paths taken during one iteration of the program.

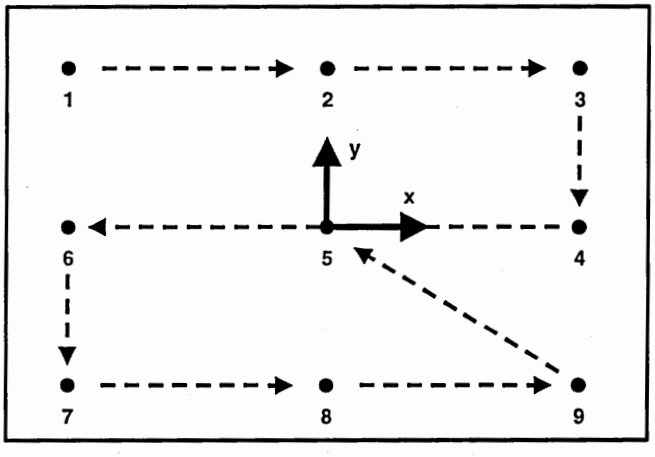

Figure 4.5: XY position repeatability test

The other three patterns have the stage approach circle #5 from the three other corners, circles #1, #3, and #7. The circles are on average 380μm in diameter, so the 10x objective was used for this test because a circle of this size fits within the 10x objective field of view. The standard was illuminated using back lighting. A cycle, defined as the completion of all four paths, takes approximately 2.5 minutes of operation across the 54 square inches of area. The largest area covered can come from inspecting an entire four-inch diameter wafer (~13 sq in). The inspection of individual parts spans less area, given that a wafer usually contains more than 20 parts. A typical part inspection lasts about ten

minutes. Inspecting smaller areas would lessen uncertainties contributed by linear encoders and thermal changes in the motors and drive spindles. Data from running the repeatability test for 25 minutes (10 cycles) was examined for XY repeatability. Figure 4.6 shows the deviations from the initial position of the center of circle #5.

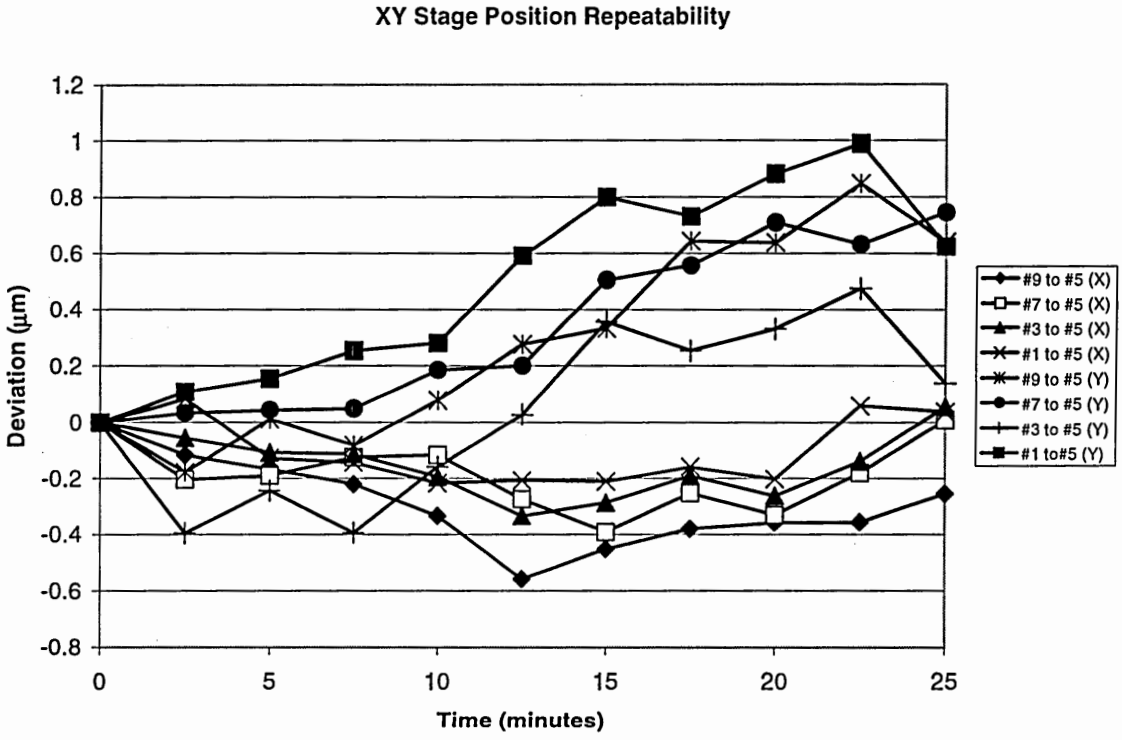

Figure 4.6: XY repeatability results

The results show that there is a slight variation depending on the direction of approach to circle #5. However, all four approaches follow similar trends in deviation with respect to time. Table 4.6 compares the data presented in Figure 4.6 to data and pass/fail criterion of the annual VIEW calibration test.

Table 4.6: XY stage results with manufacturer's pass/fail criteria

	Max Pass/Fail [μm]	VIEW Reticle [μm]	Vidicomp [μm]
Max Mean Dev X	5	2.8	3.8
Max Mean Dev Y	4	1.2	2.7
Max 3σ X	4	3.6	2.1
Max 3σ Y	3	1.8	0.7
Max Range X	Not defined	2.9	1.7
Max Range Y	Not defined	1.5	0.5

The uncertainty in the stage is determined by the maximum value found between the two axes after calculating the root sum-squares of the maximum of the means and standard deviations. Table 4.7 shows the uncertainty found by both VIEW and Vidicomp chrome grid plate testing.

Table 4.7: Stage uncertainty testing

Test	Stage Uncertainty [μm]
VIEW Standard Testing	3.69
Vidicomp	4.05

The differences may be attributed to the different size of the reticle as well as the different feature type being inspected; circles (Vidicomp) as opposed to crosshairs (VIEW). Nevertheless, the results of the stage performance testing yield lesser uncertainty values than that which are supplied by the manufacturer. The distances spanned during this repeatability test subject the instrument to more demanding

performance requirements than typical LIGA-sized inspections, making the uncertainty found in the stage quite conservative

On a smaller scale, the chrome pitch standard was used to understand the importance of taking critical measurements without translating the stage. Measurements were taken using the three objectives across three pitches of different length with and without moving the stage. The pitch was centered in the field of view, one image was captured, and the measurement was calculated by the two edges found. Next, one side of the pitch was centered in the field of view, and the edge data was captured. Then, the stage was moved to center the other side of the pitch and the edge data was saved. The results of this test are shown in Table 4.8.

Table 4.8: Small scale stage movement testing

Pitch Size [μm]	Without Stage Movement [μm]	With Stage Movement [μm]	Deviation [μm]
100	99.57	100.21	0.64
200	199.25	200.17	0.92
500	498.96	500.02	1.06

Although this study contains only a few data points, it shows that for smaller stage movements, similar to those required for inspecting LIGA microparts, uncertainty is not as large as what was recorded across the extents of the stage. This test shows an error of approximately 1μm induced by the stage movement. Therefore, 3.69μm of uncertainty is a conservative value for estimating the accuracy of the stage on a LIGA part and wafer scale.

The Z axis characteristics of the microscope are not of concern because data regarding surface topology can be acquired more precisely using the interferometer. Regardless, proper calibration is performed annually by a VIEW technician using a step height standard as shown in the earlier chapter of this report.

CHAPTER 5 : INSPECTION OF LIGA STRUCTURES

Understanding the abilities of the microscope using conventional chrome-on-glass standards is very important when developing a metrology process. A manufacturing process does not always provide specimens with simple geometry that may be inspected as easily as the calibration reticles. This section tailors the optical microscopy to typical LIGA measurement and material types that present difficulties during inspection. Tests involve the use of various lighting types and intensities to examine the effects they have on the measurement. Metallic and photoresist structures were inspected and precautions due to edge effects and part processing are presented. Suggestions on dealing with these anomalies as well as their contributions to the overall uncertainty of the measurement are given in the final section of this chapter.

5.1 Chrome Standard Pitch and Linewidth Measurements

The VIEW Voyager is equipped with three different types of lighting: coaxial (top), back, and overhead red/green LED ring lighting (Figure 5.1).

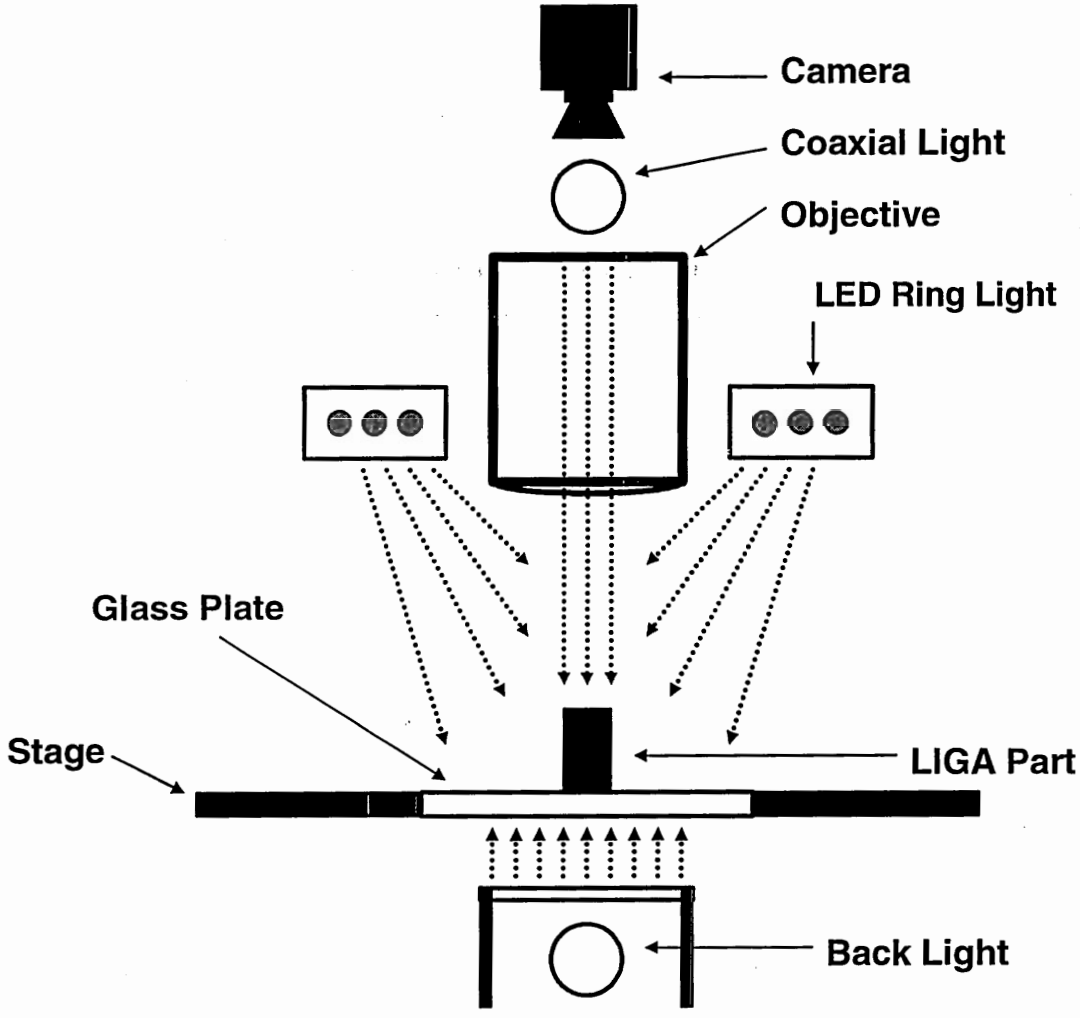

Figure 5.1: Principle sketch of VIEW Voyager lighting setup

The coaxial light shines down through the objective, above the specimen in a well-focused beam. The LED ring light surrounds the objective with a radial array of diodes, and radiates light from above and around the specimen. The back light shines through a diffusing membrane and the glass stage to illuminate the specimen from below. Each light source may be adjusted from 0 (0%) to 255 (100%) in the software. Intensities used will be noted in the form of percentages.

Two types of features on the chrome pitch standard were inspected: a linewidth and a pitch. For understanding the effects of lighting, the absolute size of the feature is not of concern. Only the differences between the measurements are of interest. The difference between the two features is illustrated in Figure 5.2 below. The upper portion of the diagram shows the grayscale principle sketch from the camera of the microscope with edge finders, and the bottom portion plots grayscale intensity profiles with respect to the dotted line on each feature [Vezzetti, et al. 1991].

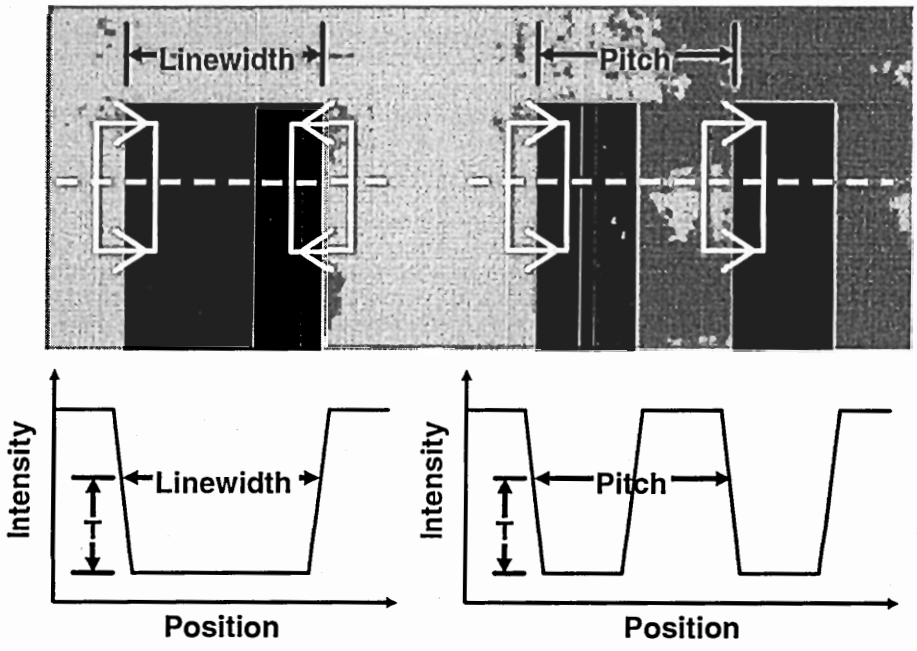

Figure 5.2: Linewidth and pitch diagrams with image intensity profiles

The main difference between the pitch and the linewidth measurement is where the edge is defined from the intensity profile of the grayscale image. Therefore, the difference in measurement between a linewidth and pitch is dependent on the intensity threshold T (Figure 5.2) at which the image processing software defines an edge

[Vezzetti, et al. 1991]. Regardless of how the intensity threshold is defined in the edge detection algorithm, the pitch measurement will remain the same across similar edge intensity profiles. This is not the case for measuring a linewidth. By looking at the image intensity profiles in Figure 5.2, if the intensity threshold T were to be decreased, the linewidth measurement would decrease as the pitch measurement would stay the same.

The intensity profile is defined by the contrast in an image and the image sharpness of the edge of a specimen. The contrast is dependant on the radiance of the specimen within the field of view and the intensity of light used to illuminate it.

The first test involved a 50µm pitch grating from the chrome pitch standard defined in Section 4.2.1. The pitch was measured across a large range of lighting intensity for both the back light and LED ring light. Coaxial lighting was disregarded. It produced unacceptable quality of the image due to the coating on the standard. The standard is used for both optical calibration and SEM calibration, so it was coated with a conductive material. The back and LED ring lights produced very similar images with the 20x objective (Figure 5.3a and Figure 5.3b).

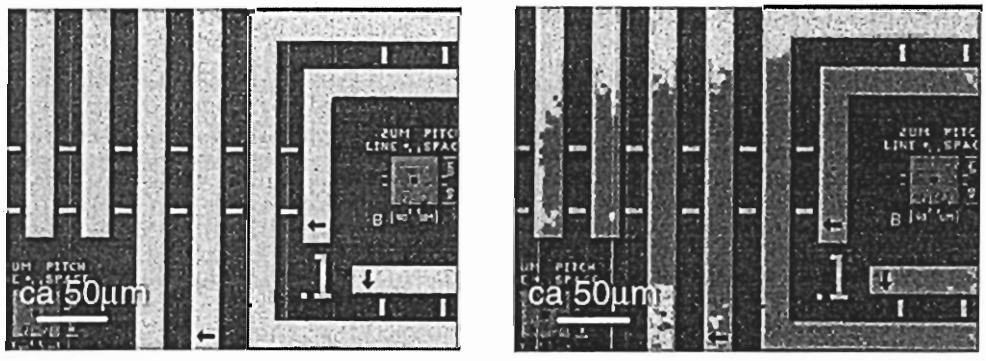

(a) (b)

Figure 5.3: 50µm chrome pitch standard illuminated using 75% back lighting (a) and 75% LED ring lighting (b)

The purpose of this test was to investigate if lighting type and intensity has an effect on the pitch measurement. Using the 20x objective, ten pitch measurements were taken at twenty percent (Figure 5.4a) light intensity. The light intensity was then increased by five percent until one-hundred percent intensity (Figure 5.4b) was reached.

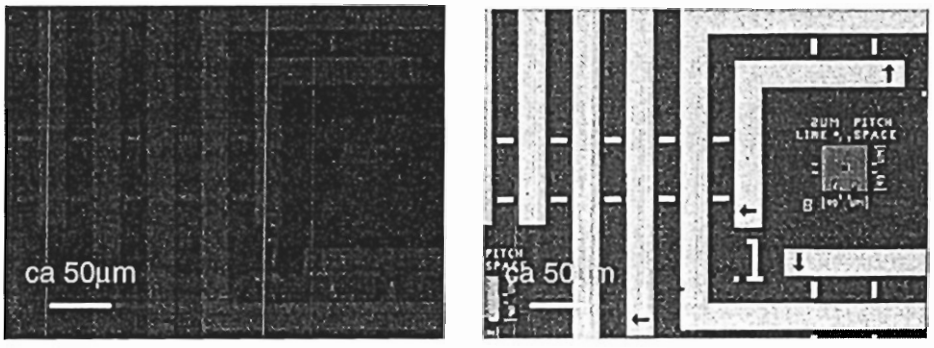

(a) (b)

Figure 5.4: Chrome pitch standard at 20% intensity (a) and 100% intensity (b) using back lighting

The mean of the deviations from the certified measurement and standard deviation at each intensity were plotted across the intensity range (Figure 5.5).

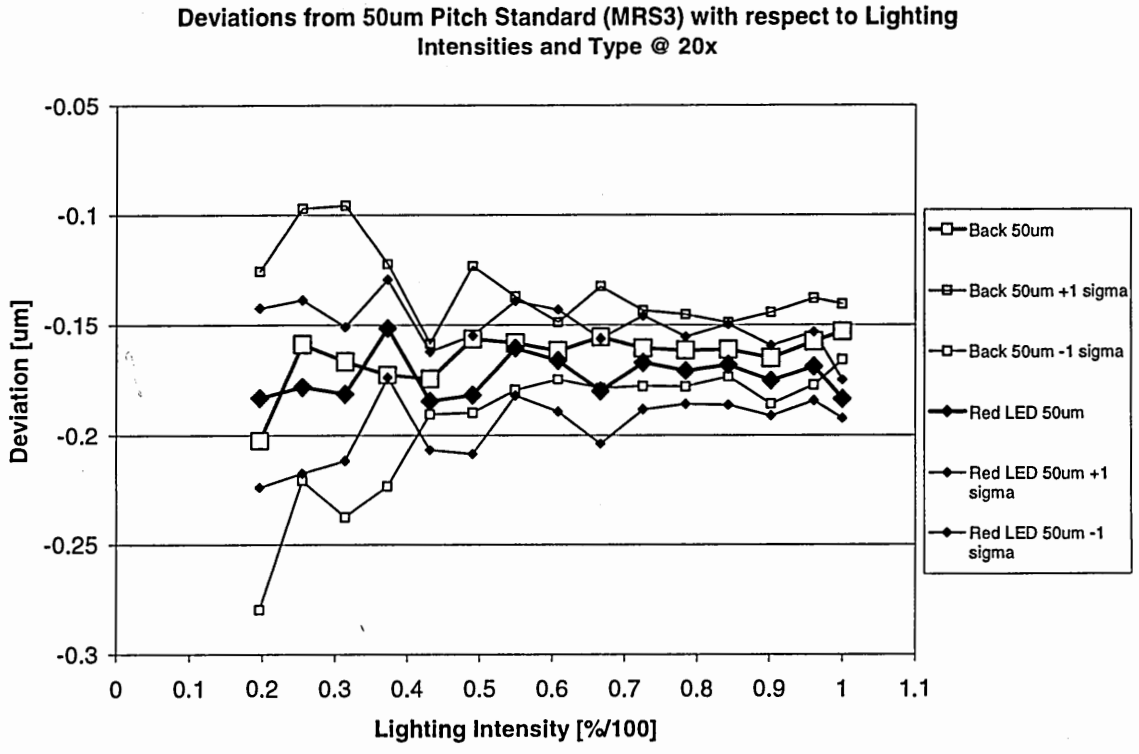

Figure 5.5: Lighting study results from the 50μm pitch standard

In Figure 5.5, the thicker lines represent the mean values of the ten measurements taken at the specified lighting intensity. The standard deviations (thin lines) show that when the lighting intensity reaches about 50 percent of maximum, the measurements become more consistent. As in all inspection processes, reproducibility is the coveted goal, so 50% or more light intensity is necessary for use. Figure 5.5 also shows that noise is reduced for light intensities greater than 50 percent. The results of averaging the measurements from 50%-100% intensity are shown in Table 5.1.

Table 5.1: Pitch standard results (Back and ring lighting: 50% - 100%)

Light Type	Mean Deviation [μm] ± σ[μm]
Back Light	-0.159 ± 0.019
LED Ring Light	-0.172 ± 0.019

The standard deviations in Table 5.1 are not those plotted in Figure 5.5, but rather the standard deviation found from all of the mean values across the lighting intensity range. The results prove that the image intensity profile has little effect on the pitch measurement. This test also validates the systematic errors found in the optics calibration section and, in turn, the notion that the microscope has the potential to measure with more accuracy than the current ± 1μm circular calibration standard, for measurements taken within the field of view.

A similar lighting test was performed on a 25μm linewidth feature to explore the effect that lighting has on a linewidth measurement. This feature was not certified. The intensity range began at forty percent and was increased by five percent until maximum lighting intensity was reached for both the back light and LED ring light. Figure 5.6 plots the mean deviation (from 25μm) for the two lighting types across the intensity range.

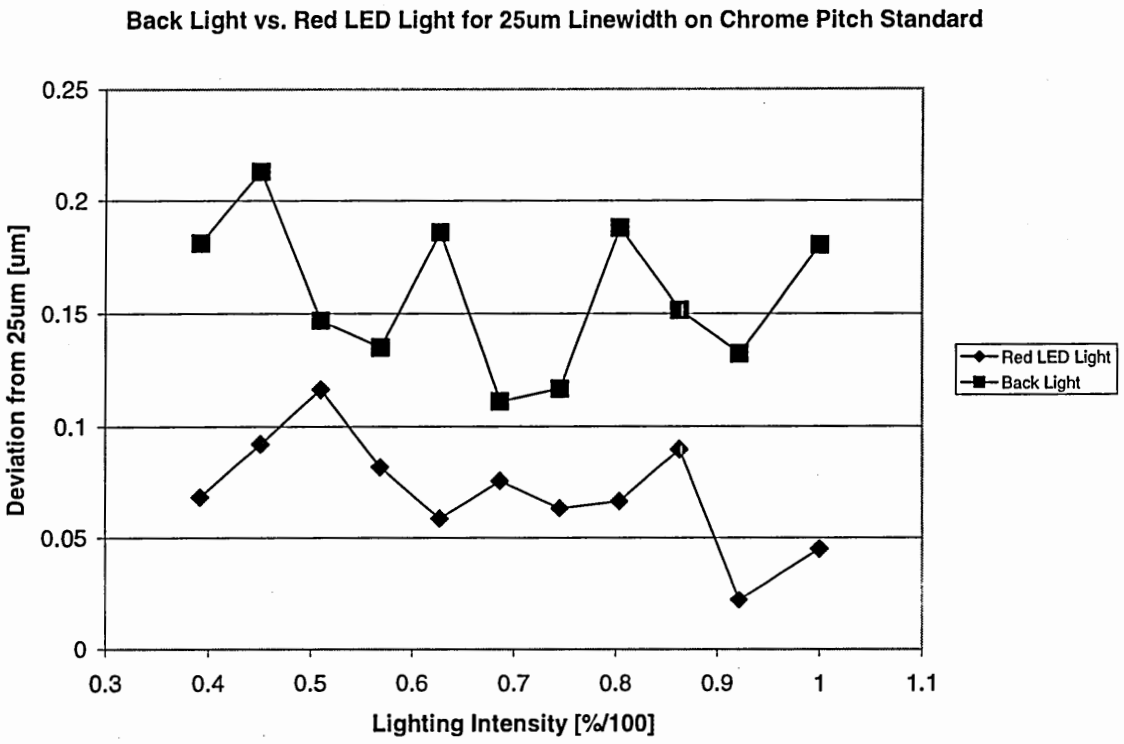

Figure 5.6: Linewidth measurements across intensities for back and LED ring lighting

Table 5.2 shows the results of this linewidth test.

Table 5.2: Linewidth test results (Back and ring lighting: 50% - 100%)

Light Type	Mean Deviation [μm] $\pm\sigma$ [μm]
Back Light	0.158 $\pm$ 0.092
LED Ring Light	0.071 $\pm$ 0.099

A difference between lighting types of 0.087μm is present for linewidth measurements. Variations in lighting condition and lighting type do not contribute to significant differences in measurement results. This is important information because the calibration of the instrument is dependent on how the standard is illuminated. Therefore,

in the case of calibrating multiple instruments with one standard, an understanding for how comparable inspection data would be across instruments can be obtained regardless of the lighting of each machine. On the other hand, although the difference is small, it is undeniably present for the inspection of chrome artifacts, and shows the need for an understanding of the effects of specimen illumination. Keep in mind that the chrome specimen has practically no topology, being 0.1μm thick on a glass plate. Thus, the makeup of this specimen, as intended, exhibits the high contrast and edge sharpness allowing for steep slopes in the image intensity profile necessary to minimize the error in edge detection.

In essence, most practical measurements of LIGA microstructures are linewidths. This is best understood by the image intensity profile across the part that is inspected. In the case of a pitch, the profile has a high-low/high-low or low-high/low-high nature in which the two edges are defined across descending/descending or ascending/ascending slopes, respectively. Linewidths are defined by a high-low/low-high or low-high/high-low profile having opposing slopes. For instance, measuring the circumference of the inner diameter of a cylindrical specimen would be similar to that of a linewidth. Figure 5.7 shows the intensity profile of a cylinder, of arbitrary thickness, across its diameter.

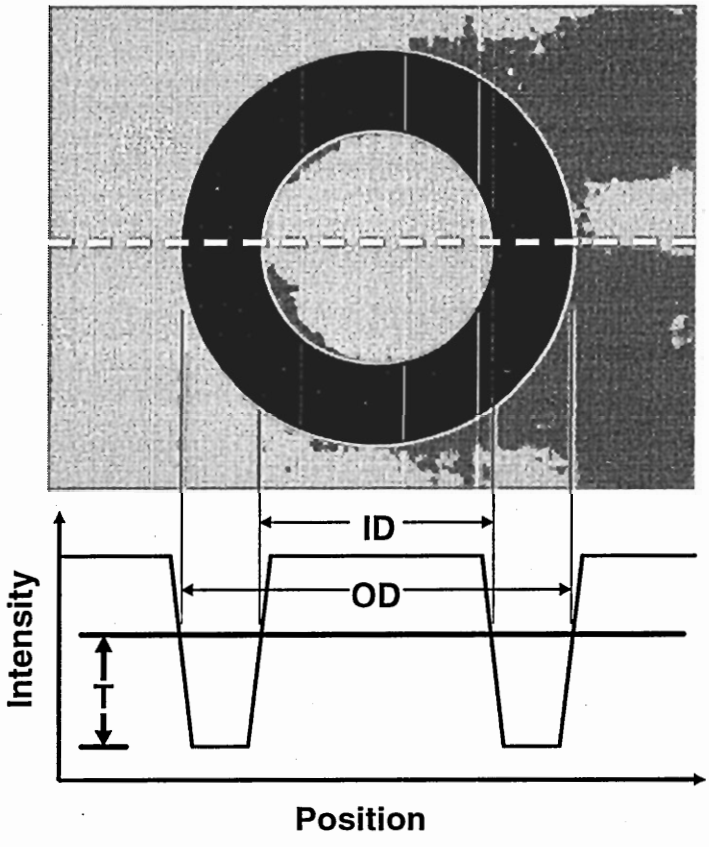

Figure 5.7: Intensity profile for inspecting a cylinder

Measurements, other than pitches, that do not depend on lighting type and intensity are center points defined by circular edge detection. Therefore, when measuring the location of the center of a circle, or the center-to-center distance between circles, there is no need to understand the effects of lighting.

Regarding the difference found between the back and ring lighting linewidth measurements for chrome reticles, the question regarding which measurement is correct still remains. By visual inspection, the answer is not apparent, so more specimens must be introduced, and tested similarly.

5.2 Stainless Steel Gauge Block Testing

The LIGA process is acclaimed for its ability to produce high aspect ratio microstructures. For the first case study, a 150μm NIST traceable stainless steel gauge block (certified to ±0.04μm) was used to most closely emulate a LIGA processed metal structure while being a certified width in one dimension. This specimen was encased in clear epoxy polymer and then planarized by lapping and polishing procedures following the current in-house LIGA process guidelines. Once the part was released from the epoxy, it was subjected to inspection under a range of suitable lighting intensities and lighting types offered by the microscope. Figure 5.8 shows the released gauge block under all three lighting types.

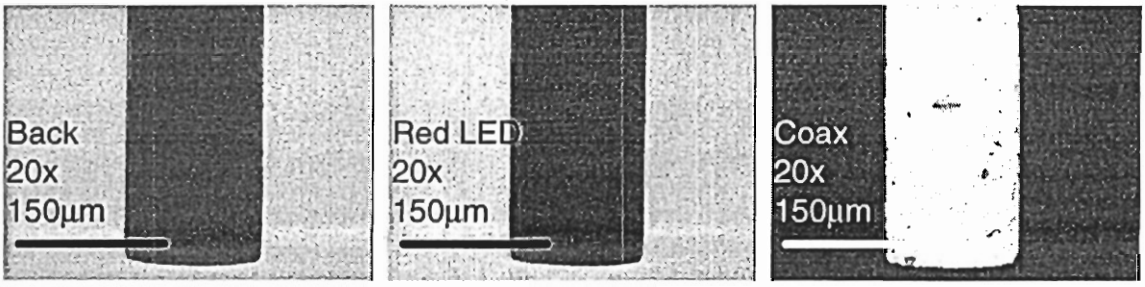

Figure 5.8: Released gauge block under different lighting types

Before presenting the measurement results, an understanding for the edge detection capabilities of the microscope is needed. There are many options available in the software to aid in finding the correct edge when obstacles are present. Once a finder (Figure 3.4) is placed on an edge, the arrows designate the direction in which the algorithms detect

edges. The user may specify a "rising" (Figure 5.9a) or "falling" (Figure 5.9b) edge to detect, meaning "dark to light" and "light to dark" grayscale transitions, respectively.

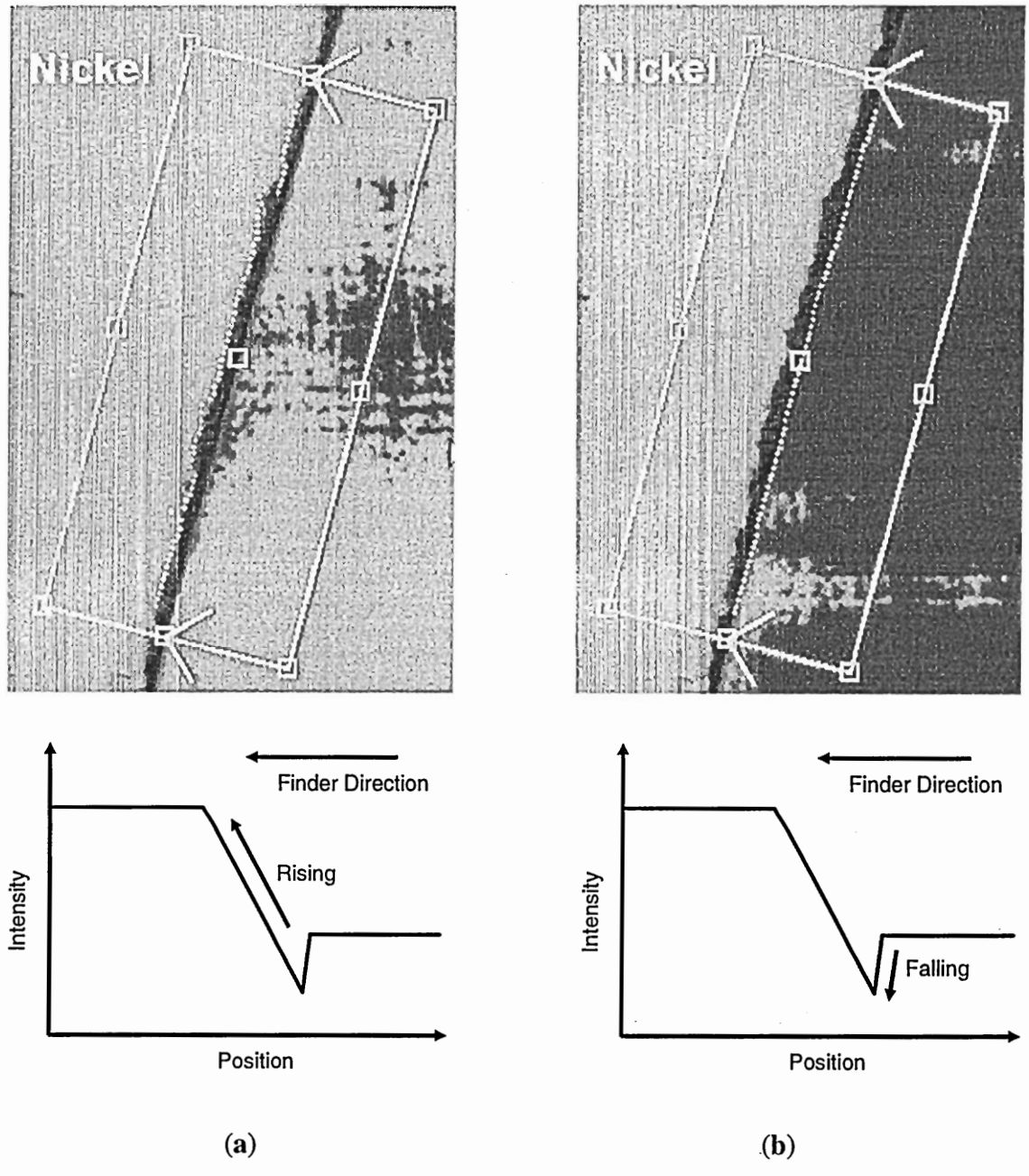

Figure 5.9: Rising (a) and falling (b) edge detection across the edge of a LIGA nickel part with corresponding grayscale intensity profiles

As shown in the figures, there is a visible difference between the edges that are defined by the edge detection in this instance. This situation is brought about by a combination of surface roughness, edge topology, and the high aspect ratio of structures created by the LIGA process. The surface roughness and edge topology in this example come from the lapping and polishing steps of the process. The uncertainty attributed to a high aspect ratio is due to the nature of the sidewalls produced by the process. Small deviations from perfectly normal, due to effects discussed earlier, on the order of 0.1 degree may be realized. Figure 5.10 shows a detailed look at the edge detection occurring in Figure 5.9 from a cross-sectional point of view.

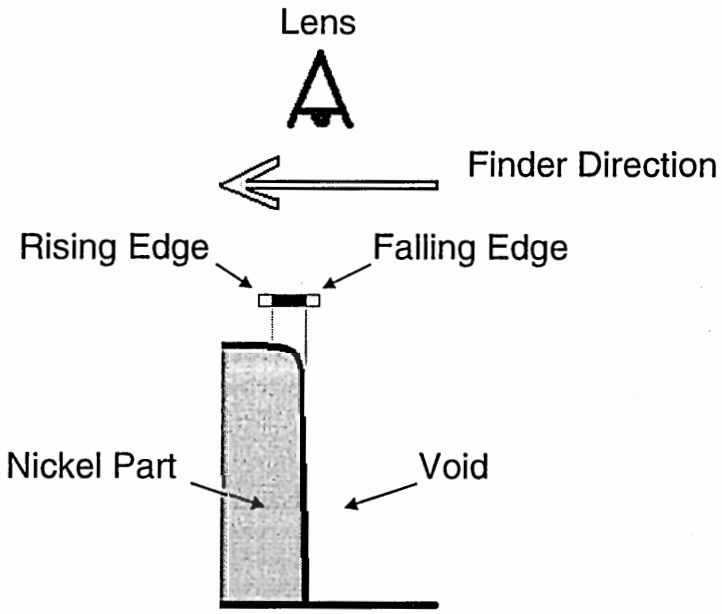

Figure 5.10: Principle drawing of the edge detection of a cross section of a high aspect ratio part with exaggerated artifacts

The same lighting test that was performed on the pitch standard was used on the released gauge block. The coaxial lighting type was added to the test since an acceptable image could be produced. The polished surface of the gauge block had much more radiance than the surrounding glass stage, causing a bright field on the gauge block, and a dark field on the glass stage. Because of the focused beam of the coaxial light, the range was much larger than the back and LED ring lighting.

The results of the lighting test performed on the embedded gauge block are shown in Figure 5.11.

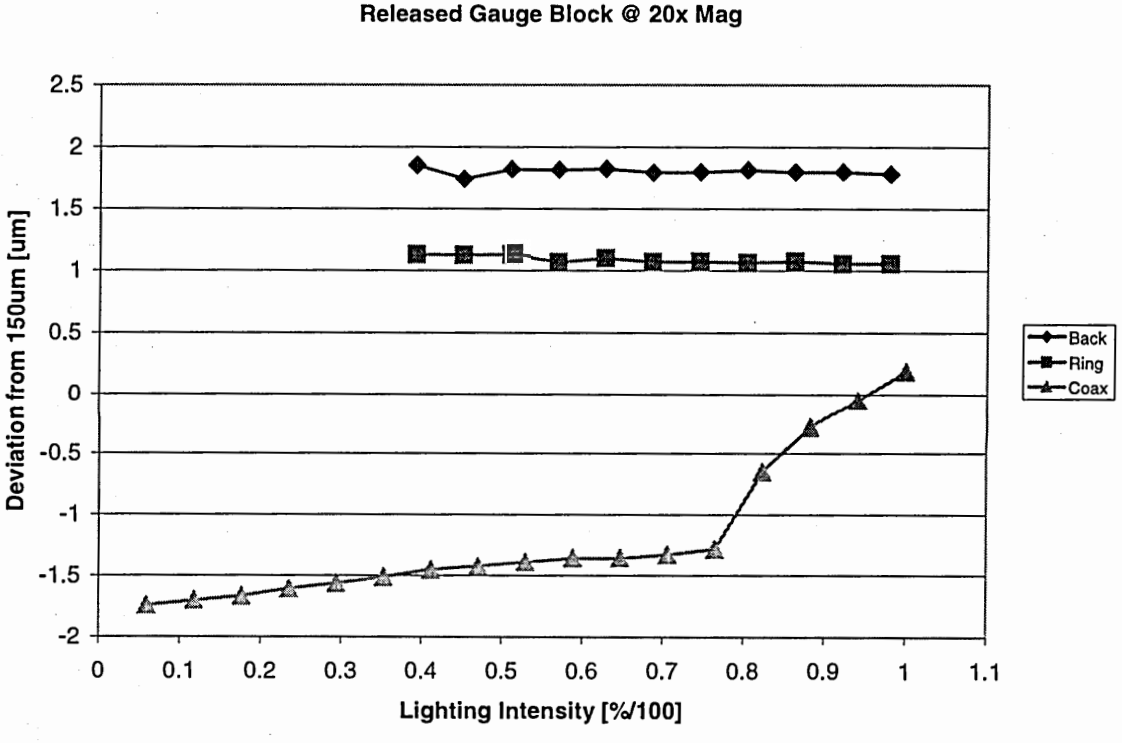

Figure 5.11: Lighting study on embedded gauge block

A much larger difference in size, on the order of 0.72μm, is seen between the back lighting and the LED lighting. Standard deviations exhibit the same trends as seen in the pitch standard test across lower light levels due to insufficient contrast and edge sharpness. The difference from the nominal width of 150 ±0.04μm can be attributed to the LIGA lapping and polishing procedures (Figure 5.12).

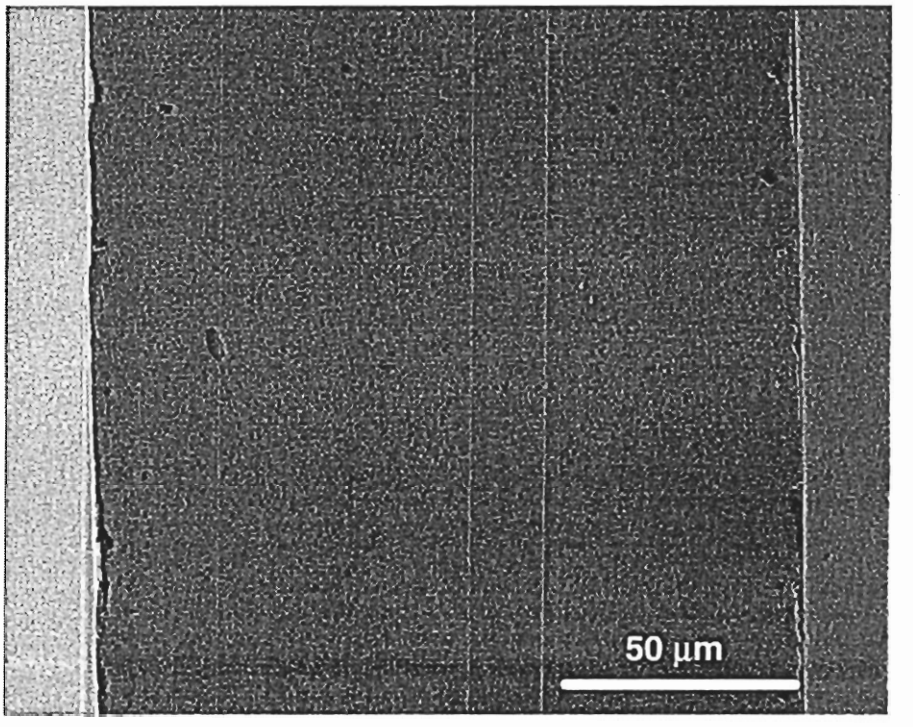

Figure 5.12: SEM image of a top view of stainless steel gauge block

The measurements taken from the coaxial lighting can be discarded when looking at the detected edge during inspection. The coaxial light tends to illuminate the surface roughness of the part, skewing the edge detection. Most measurements with the coaxial light have a material-side bias (Figure 5.9a), since it does not sense the outermost boundary of the part (Figure 5.9b). This "filleted" edge topology is seen when inspecting

both electroplated parts and photoresists. Another undesirable effect of the coaxial light is the large change in measurement as the intensity exceeds 75%, as seen in Figure 5.11. This is the forewarned blooming effect caused by flooding the camera with too much light. Blooming is not a quality inherent of only the coaxial light. The intensities available for the other two lighting types are set so they do not bloom the sensor. These intensities could be adjusted so that this blooming effect is seen for the back and ring lights. However, all equipment in this study is maintained to be as available commercially.

The 0.72μm difference between the linewidth measurements taken with the back and ring lighting shows that there is a systematic difference in single edge detection of 0.36μm when using these light types. The backlit measurements are larger than those taken by the ring light, having a bias towards the void-side (Figure 5.10).

An explanation for the submicron difference in measurement between the ring light and the back light could not be found by eye in the images at 20x magnification (Figure 5.8). However, the effects of the LED lighting seem to be more apparent when viewing the gauge block with the 10x objective. Figure 5.13 shows the gauge block at 10x magnification illuminated by back lighting and LED lighting.

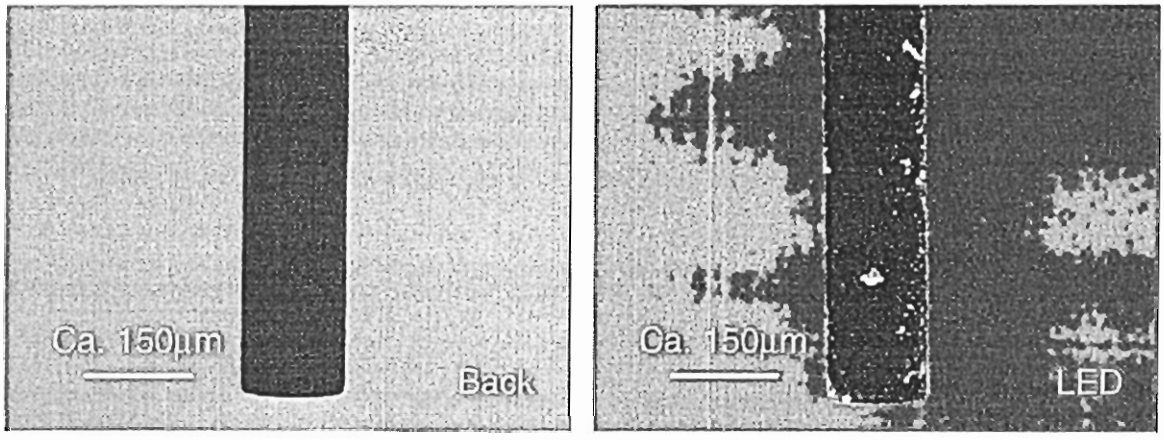

Figure 5.13: Released gauge block at 10x magnification, back light (left) and ring light (right)

The LED ring light illuminates the specimen from the top and side, illuminating the scene for the lens by reflecting light from the specimen and the field. The edge topology and surface roughness create a bright boundary around the specimen that hinders the ability for the edge detection algorithm to capture the outermost edge. This edge lighting effect is not as pronounced when using the 20x magnification. This is due to the ability of the objective to retrieve light at higher magnification and higher numerical aperture. Therefore, the LED light may be omitted for the same reason as the coaxial light. To verify that the previous statements, the light intensity study was performed using the 10x objective with the back and LED illumination. Figure 5.14 shows the mean measurement difference for the 150µm linewidth between the two lighting types for inspection at 10x and 20x across lighting intensities.

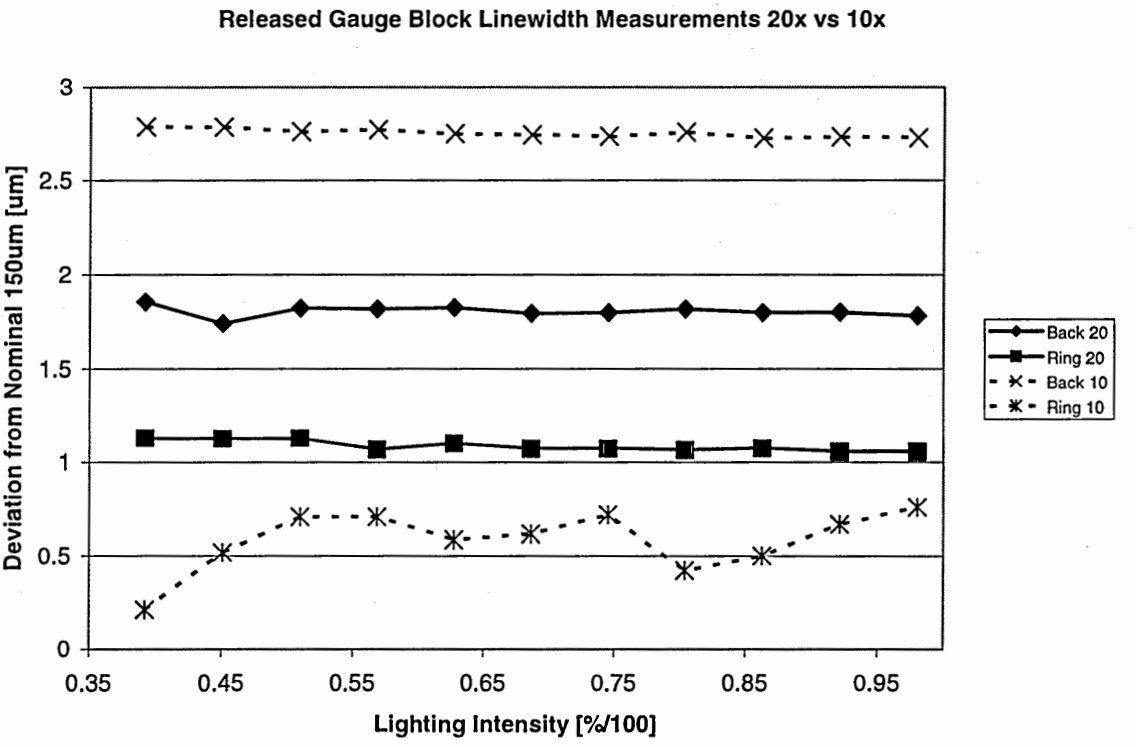

Figure 5.14: Linewidth measurements across lighting intensities for back and ring lighting at 10x and 20x magnification

The graph shows that measurements for both the 10x and 20x backlighting measurements are larger than their LED ring-illuminated counterparts. The 20x data is enveloped by the 10x data, suggesting a more accurate measurement resulting from the higher resolution of the 20x lens. Table 5.3 shows the results from this lighting test.

Table 5.3: Deviations from 150μm for the released gauge block across lighting types and magnifications

Objective	Back Lighting Mean $\pm\sigma$ [μm]	LED Lighting Mean $\pm\sigma$ [μm]
20x	1.80 $\pm$0.06	1.09 $\pm$0.06
10x	2.75 $\pm$0.05	0.58 $\pm$0.49

The outlier in the results is the standard deviation of the LED ring lighting measurements at 10x magnification. This demonstrates that when rough edge topology is present, the measurement is less consistent when illuminated by the ring light. At higher magnification, this effect is not apparent, however present. Therefore, to achieve the correct measurement, back lighting is recommended for released metallic parts and chrome masks.

A disadvantage of using the back light is that the image is created from light being projected from beneath the part. Small particles or defects close to the inspection surface may create a shadowing effect that blurs the sharp contrast of the edge. To keep this problem limited, careful cleaning and processing procedures are mandatory.

5.3 Photoresist Inspection

Aside from the chrome mask and the released metallic parts, the gold mask and the mold should also be inspected. These two steps define the quality of the final part. The gold mask may be used for multiple exposures, so inspection is necessary to verify its correctness for producing parts and to track any changes occurring over its period of use. Inspecting the mold provides information on the characteristics of the synchrotron and scanner, such as beam divergence and alignment [Menz, et al. 2001]. Mold inspection can also uncover defects that may stem from mask defects found in a region that was not accessible with the VIEW microscope. This data also gives insight to discrepancies and

variability occurring in the photoresist processing such as development times, development baths, and UV and X-ray doses.

The photoresist structures, such as SU8 and PMMA, are transparent polymers bonded to metallized wafers. The metals, such as aluminum, gold, and titanium, are highly radiant. Back lighting is not an option since light cannot pass through the wafer and metallic layers. The LED ring lighting is unable to create acceptable contrast for edge detection. This is attributed to the angle at which the light is directed from multiple sources surrounding the specimen, the radiance of the metallized wafer surface, and the transparent structure. The coaxial light is the only lighting type that produces an acceptable edge. Figure 5.15 shows the coaxial illumination setup for photoresist structures.

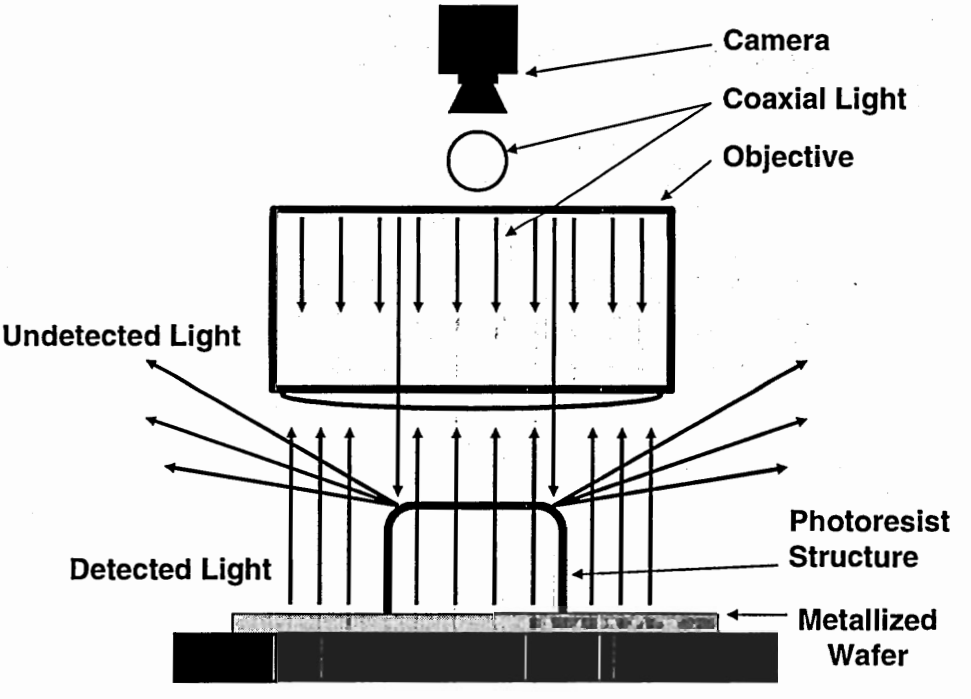

Figure 5.15: Setup of photoresist inspection

The image shows little contrast between the photoresist structure and the substrate due to the inability of the transparent photoresist structure to diffuse the light radiating from its metallized backing. A fine dark line is present defining the edge of the structure. The rounded shape of the edge reflects light away from the camera, creating the dark line. Figure 5.16 shows an SU8 photoresist structure under inspection.

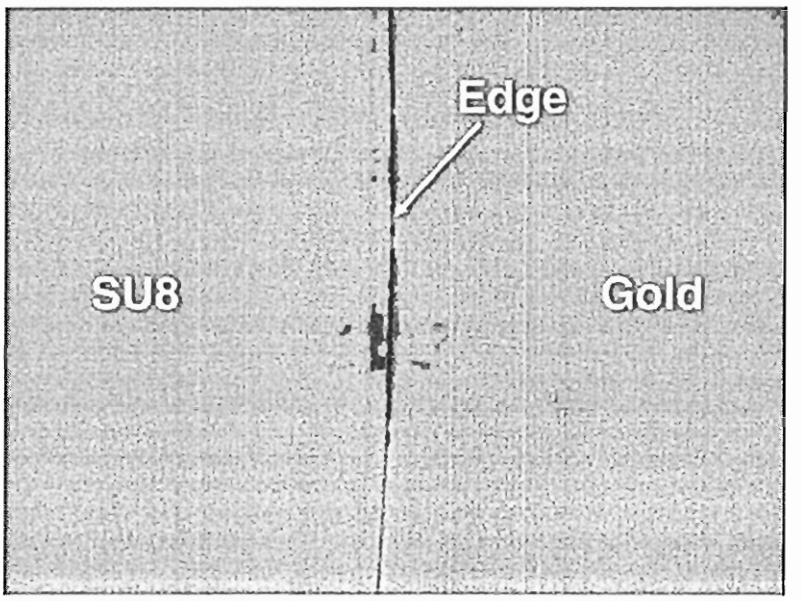

Figure 5.16: SU8 photoresist at 40% coaxial illumination

Figure 5.17 shows an SEM image of the rounded edge of the SU8 structure.

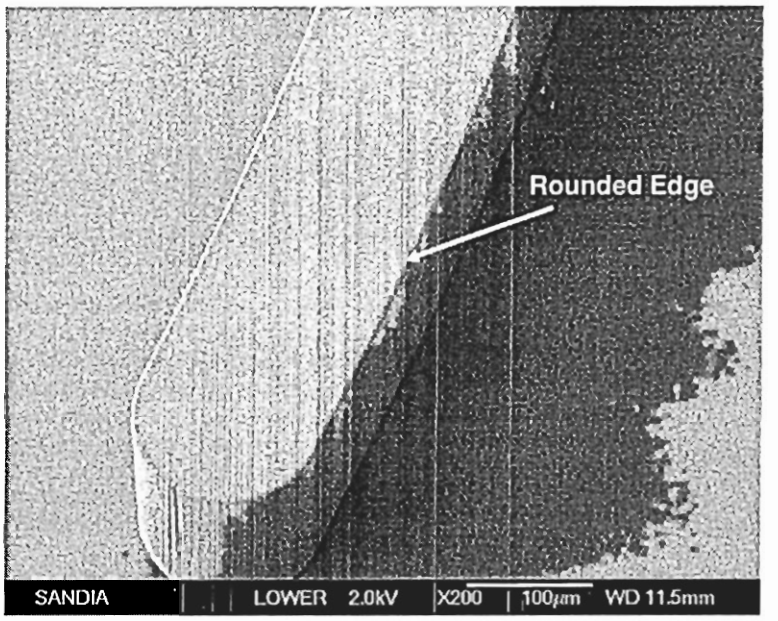

Figure 5.17: SEM image of SU8 specimen

Frequently this edge is encountered when inspecting positive and negative photoresists. The thickness of the dark line varies with magnification. The dark line of an SU8 sample was measured five times using each magnification: 10x, 20x, and 50x. The focus was fixed once the edge appeared sharp in the image. Table 5.4 shows the results of the test by mean and standard deviation of the measurements.

Table 5.4: Width measurements of an SU8 edge at different magnifications

Objective	Edge Width $\pm$ σ [µm]
10x	2.89 $\pm$ 0.05
20x	2.07 $\pm$ 0.05
50x	1.31 $\pm$ 0.12

The results from Table 5.4 show that the dark line at the edge of the specimen is larger at lower magnifications, and the measurement becomes less consistent at the highest magnification. The depth of focus of the objective plays an important role in the explanation for this effect. The depth of focus refers to the distance away from the focal plane of the lens in which an object may be in focus. The focus refers to the sharpness of the object/feature under inspection and is at the discretion of the operator. Therefore, edges that have steep topology extending beyond the depth of focus bounds of the objective would pose more difficulty in achieving sharpness. The steep slope of the structure within the depth of focus causes a blurring effect at the outside edge of the dark line. Hence, the edge detection is less consistent as in the case of the 50x objective.

Initially, one would think that examining the thickness of the photoresist edge in the inspection does not make a lot of sense. The only edge that should be of concern is the outer edge of the structure. Due to the nature of the transparent high-aspect ratio structure bonded to a highly radiant wafer surface, the obtaining enough contrast for image processing is challenging. Often times the outer edge is unable to be detected, although present. Figure 5.18 shows an image of PMMA photoresist under the best achievable lighting conditions. Looking closely at the edge, the dark line is barely visible and undetectable to the edge detection algorithm. The contrast between this outer, "void-side" edge and the titanium field does not produce a large enough grayscale gradient to define the edge consistently.

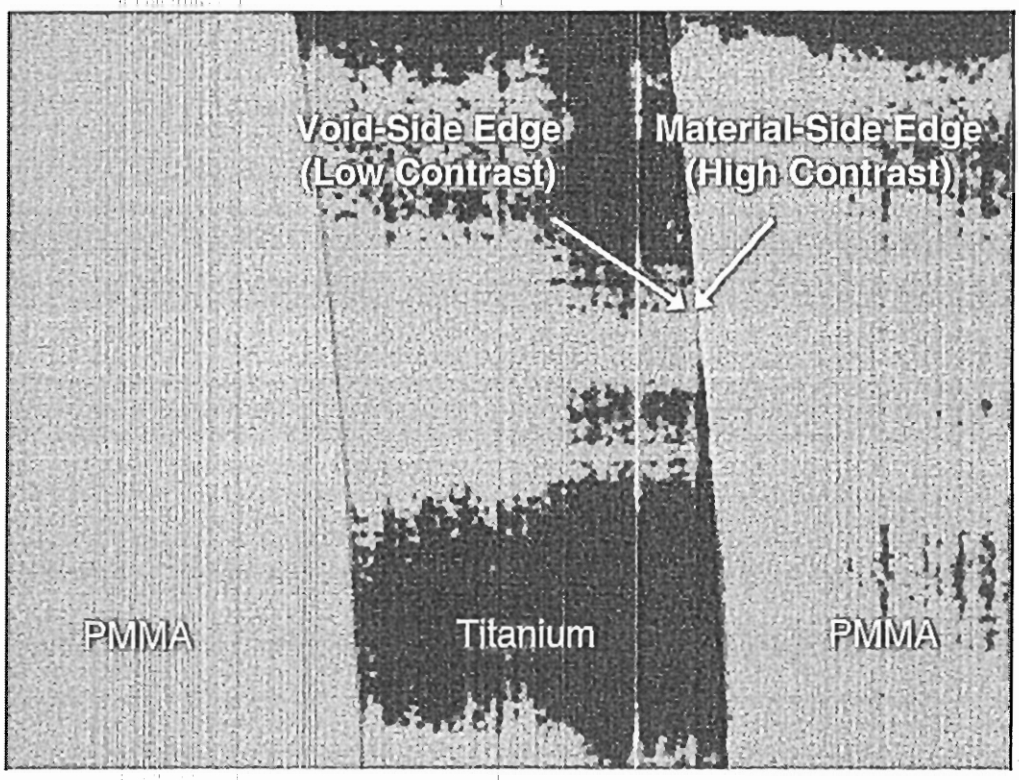

Figure 5.18: PMMA mold with undetectable outer edge

The inside "material-side" edge of the PMMA, on the other hand, is always present and well-defined. The importance of understanding the thickness of the dark line under different magnifications is to enable the use of a correction value to add or subtract to the measurement. By the fidelity of the manufacturing process, the amount that the edge varies in thickness is minimal in comparison to the to the uncertainty added the measurement when measuring the inside or outside depending on its availability. Therefore, it is necessary to consider a material-side and void-side convention for edge detection bias. A more consistent approach to inspecting photoresist structures would be to inspect the material-side of the dark line representing the edge and implementing a correction value. This correction value is found by measuring the width of the edges at

random locations across a mold or photoresist and calculating a mean and standard deviation from the accumulated data. The mean of the data will represent the value to either be added or subtracted to the measurement per edge, and the standard deviation will be added to the uncertainty of the photoresist inspection. Special precautions have to be taken into consideration before using this correction. The width measurement is either a linewidth or a channel depending on if the specimen is an SU8 mask or a PMMA mold, respectively. This must be understood prior to using the correction value. For instance, a linewidth on an SU8 mask would add the correction value to each edge whereas the correction value would be subtracted for the PMMA mold. Figure 5.19 shows the correction for a linewidth measurement for a typical SU8 and PMMA structure.

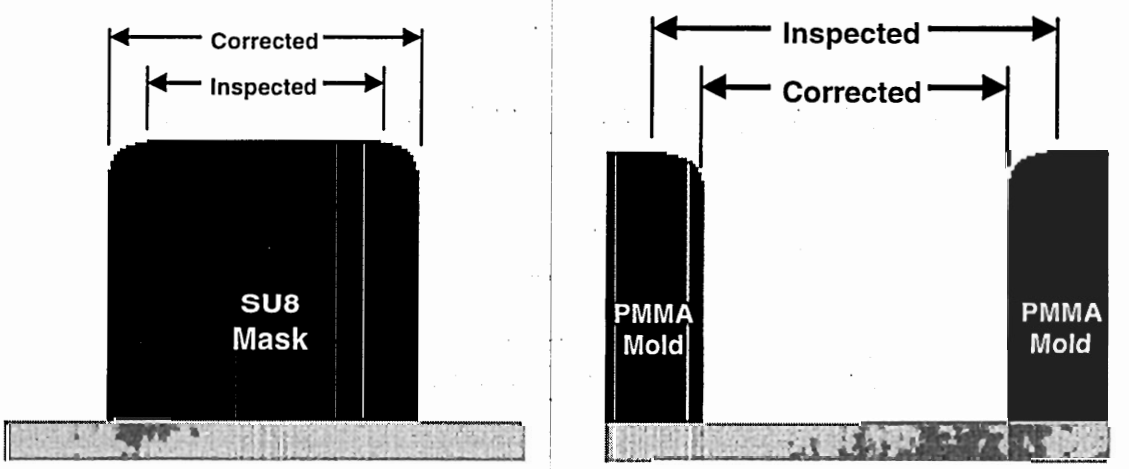

Figure 5.19: Corrected inspection for SU8 (linewidth) and PMMA (channel) structures

The use of the correction value is for cases where it is too difficult to detect the desired outer void-side edge. This induces more uncertainty in the measurement for photoresist structures in comparison to released parts and chrome masks.

A 150μm SU8 linewidth structure, not traceable to NIST certification, was prepared for the lighting examination similar to that of the gauge block. The specimen is shown in Figure 5.20.

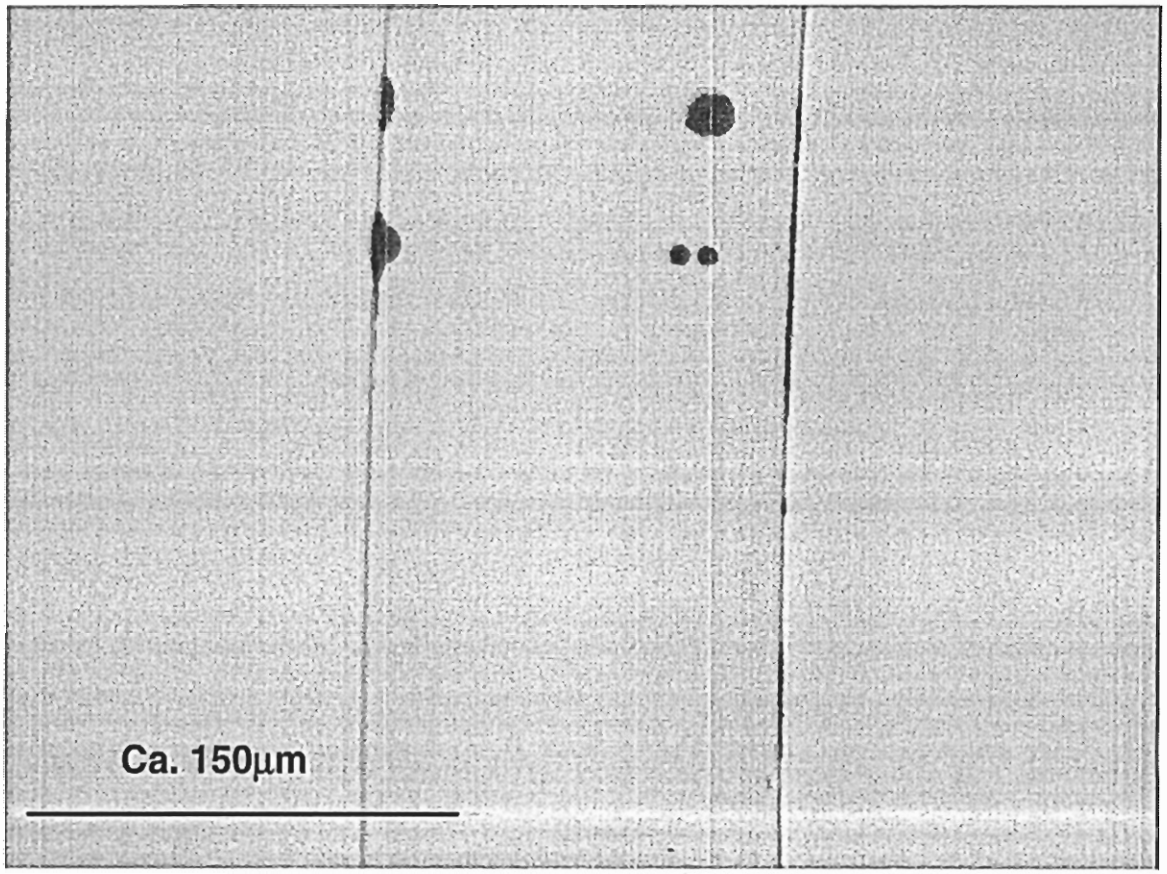

Figure 5.20: SU8 linewidth specimen under 60% coaxial illumination at 20x magnification

The coaxial light intensity was varied in five percent increments from 1% to maximum intensity for the 20x objective, and from 1% to 75% for the 10x objective. Ten measurements were taken at each intensity at the void-side edges of the structure.

Intensity exceeding 70% failed to produce an edge due to oversaturation. Figure 5.21 shows the linewidth measurement for both the 10x and 20x objectives.

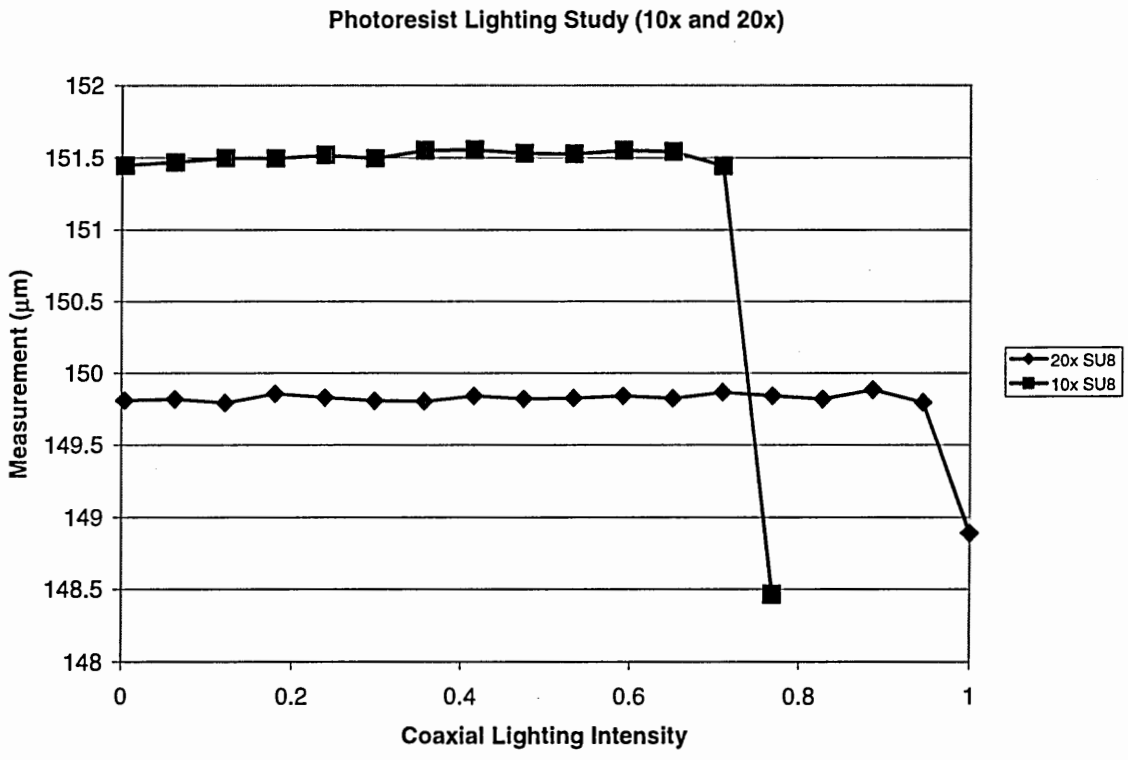

Figure 5.21: Measurement change with respect to lighting intensity for photoresist inspection

The point at which the measurement becomes altered by too much light is quite obvious. The outliers at the end of the intensity ranges were removed for statistical calculations. Table 5.5 shows the results from the intensity study at both magnifications.

Table 5.5: Results from the photoresist lighting intensity study

Objective	Mean $\pm\sigma$ [μm] (intensity)
10x	151.51 $\pm$0.04 (1%-70%)
20x	149.83 $\pm$0.02 (1%-95%)

The results are stable across most of the intensity range. This is quite encouraging when comparing measurements taken at various lighting intensities, because additional uncertainty is small.

Since coaxial illumination is the only option available for illuminating the photoresists, the SEM was used to verify the measurement. Measuring specimens with an SEM does not necessarily ensure greater accuracy because the measurements are processed using the same type of image processing. The advantage of using the SEM is its ability to inspect specimens allowing arbitrary, non-stop zoom. Using the SEM, the 150μm linewidth may be observed within the field of view at 600x magnification. This translates into 0.154μm/pixel in the SEM as opposed to 0.552μm/pixel at 20x magnification with the optical microscope. Figure 5.22 shows the SU8 structure in the SEM.

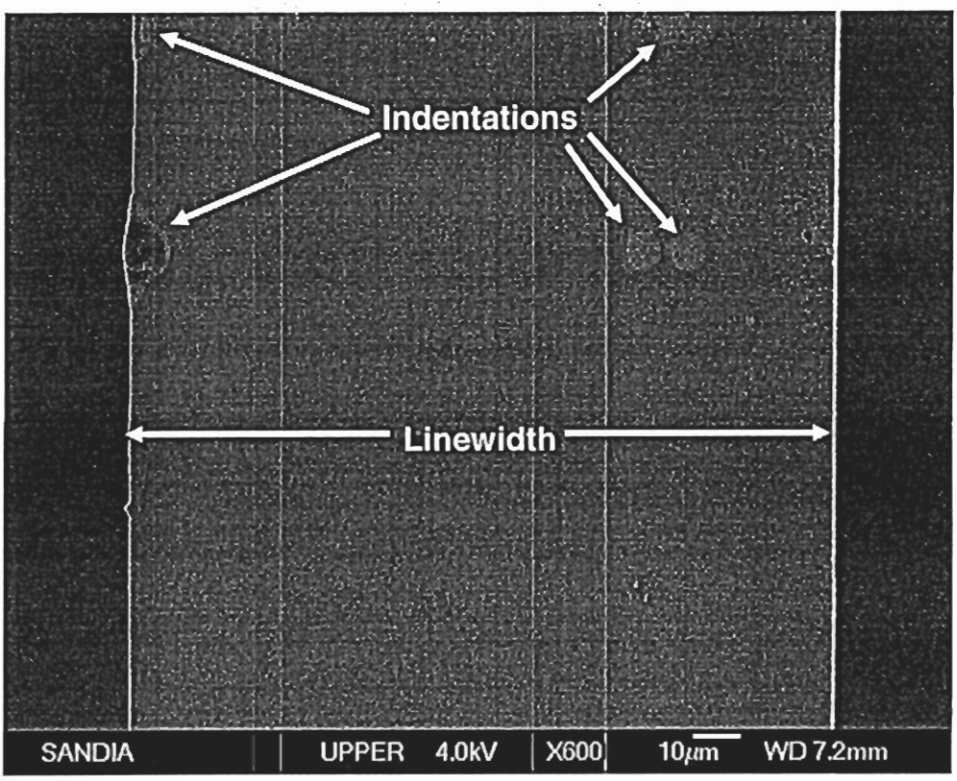

Figure 5.22: SEM image of SU8 structure

Along with the SU8 specimen, the pitch standard was placed in the SEM for calibration. Measurements were taken across three 50μm pitches under the same inspection settings that were used for the SU8 sample. Precautions were taken to account for the slight charging seen on the right edge of the structure [JEOL 2003]. This involved taking two types of measurements. The first measurement detected the material-side edges and the second detected the void-side edges. These measurements gave a range of where the true measurement lies after the correction factor, the product of the certified pitch measurement and the measured value, from the pitch standard was applied. Table 5.6 shows the results of measuring the pitch standard, calculating the correction factor, and the measured and corrected values across the SU8 linewidth structure.

Table 5.6: SEM measurement results

Measurement	Value
150μm pitch from standard	149.98μm (certified)
SEM 150μm pitch measurement	154.69μm
Correction Factor	0.969
150μm SU8 structure (material-side)	153.22μm (as measured)
150μm SU8 structure (material-side)	148.55μm (corrected)
150μm SU8 structure (void-side)	155.13μm (as measured)
150μm SU8 structure (void-side)	150.41μm (corrected)

The results show that the 20x measurement of the optical microscope falls within the bounds of the SEM measurements. This reinforces the recommendation to use an objective that maximizes the feature within the field of view, to take advantage of higher resolution. The SEM data verifies that the optical microscope is achieving reasonable results using the coaxial light on photoresist structures.

5.4 LIGA Inspection Uncertainty

The purpose for studying the optical inspection of the various structures of the LIGA process is to assess the amount of uncertainty in each measurement. A single value of that envelopes inspection uncertainty across all LIGA metrology situations is not an effective option. As explored, there are many factors that contribute to the uncertainty in each measurement. The overall measurement uncertainty will be calculated similar to a

combined standard uncertainty using a root sum-squared (RSS) method [NIST 1994, NIST 2003].

$$U_{inspection} = \sqrt{U_1 + U_2 + ... + U_n} \tag{5.1}$$

Table 5.7 shows all of the uncertainty components studied in chapters four and five as well as a value or explanation on how the value may be determined.

Table 5.7: Uncertainty components of LIGA inspection

Uncertainty Component	Value
U_{optics}	1μm (chrome calibration standard)
U_{stage}	3.69μm (95% confidence)
$U_{repeatability}$	0.14μm (95% confidence)
$U_{released\ parts}$	0 (as if measuring a chrome part)
$U_{photoresist}$	σ_{edge} (after bias for material-side inspection)
$U_{back\ lighting}$	< 0.1μm
$U_{LED\ ring\ lighting}$	< 0.1μm
$U_{coaxial\ lighting}$	< 0.1μm
$U_{temperature}$	Length/Material dependent
$U_{lapping/polishing}$	Must be characterized by optical profiler or SEM

The uncertainty in the optics is derived from the chrome calibration standard. The stage uncertainty was found using the high resolution grid plate taking the root sum-squared value of the maximum mean deviation and twice (95% confidence) the maximum standard deviation. The repeatability was calculated by twice the average

standard deviation of any arbitrary test measuring the same feature multiple times. After understanding that the back lighting option defines the correct edge amongst lighting types for chrome and released metal structures, the uncertainty contribution from this material type is covered by that of the calibration standard for the optics. When inspecting photoresist structures, the standard deviation of numerous edge thickness measurements is the uncertainty component. The purpose for uncertainty components under different lighting types is for comparing measurements taking at different intensities. These components were calculated by the range of the mean inspection values across the intensities during the lighting tests. For instance, if a released part was inspected once with 50% back lighting and then again using 75% backlighting, the measurements may vary by 0.1μm. Assessing this level of uncertainty is difficult because it nears the repeatability of the microscope.

Uncertainty due to temperature is dependent on the material properties of the specimen. This value should be treated carefully because it is length dependent. The temperature uncertainty contribution on a field of view measurement or a measurement involving the stage is significantly less than the uncertainty contribution of the stage and optics.

For example, a 500μm photoresist linewidth structure, having the largest coefficient of thermal expansion for the LIGA materials, would expand 0.077μm (0.035μm per edge) if exposed to two degrees of temperature change. This value is insignificant in comparison to the optics calibration and repeatability of the microscope for a measurement not involving stage movement.

On the other hand, a measurement across a PMMA mold (~76mm) may contribute to as much as a 11μm difference for two degrees of temperature change. This effect is quite significant, and must be taken into account during this level of inspection.

5.4.1 Feature Inspection of a PMMA Mold

Calculating the inspection uncertainty of the width measurements for spring arm channels from a PMMA mold would involve several steps. After choosing the 20x objective, the thickness of the dark line is inspected at several locations where it is available. The mean and standard deviation of this data is then calculated. Next, the inspection program is setup to capture the material side of the dark line representing the edge of the PMMA. Coaxial lighting intensity is set between 1% and 95% to produce acceptable contrast. After completing the inspection program, the twenty linewidth measurements must be corrected and the inspection uncertainty calculated. The PMMA that surrounds the arms is approximately 700μm wide before a surrounding channel is encountered. In a simplified scenario, the thermal expansion occurring at the top surface of the structure is considered to be uniform across the 700μm width although the PMMA is fixed to the metallized wafer. The room was at 23.8 $\pm$1 degree Celsius during inspection. The coefficient of thermal expansion of the PMMA is 77 μm/m-C and is applied to the variability of the temperature control of the room. The data from this inspection is given in Table 5.8.

Table 5.8: PMMA linewidth inspection and uncertainty data

Inspection Data	Value [μm]
Edge Thickness (10 samples)	2.03 ± 0.48 (95% confidence)
Linewidth Data (20 samples)	156.45 ± 2.80 (95% confidence)
Adjusted Linewidth Data (bias = -4.06μm)	152.39 ± 2.80 (95% confidence)
U_{optics}	± 1 (chrome calibration standard)
$U_{repeatability}$	± 0.14 (95% confidence)
$U_{photoresist}$	± 0.96 (95% confidence for two edges)
U_{stage}	0 (FOV measurement)
$U_{coaxial\ lighting}$	0 (no data to compare to)
$U_{temperature}$	± 0.54 (from ± 1 degree Celsius)
$U_{lapping/polishing}$	0 (none performed)

Therefore, calculating the combined standard uncertainty of the four contributing components, the PMMA mold inspection would have an inspection uncertainty of ± 1.49μm at 95% confidence associated with the adjusted linewidth data. The uncertainty components that were not used in this example are easily incorporated for cases dealing with non-FOV measurements, comparisons between data sets taken at different lighting intensities (same light type), and structures that endure lapping and polishing procedures.

CHAPTER 6 : DATA ANALYSIS SOFTWARE

The Voyager system has the ability to acquire large amounts of data. Post-processing the data with commercially available software packages has been a very time-consuming task. However, by coupling the commercially available software with software toolboxes developed for this work, post-processing time has been greatly reduced, and data analysis has become more user-friendly.

6.1 VIEW Metrology Software (VMS)

The *VIEW Metrology Software* (VMS) allows the user to create inspection programs, or macros, that allow measurement locations, measurement types, and data output to be customized. A typical scene from the VMS GUI is shown in Figure 6.1 along with comments indicating window functions.

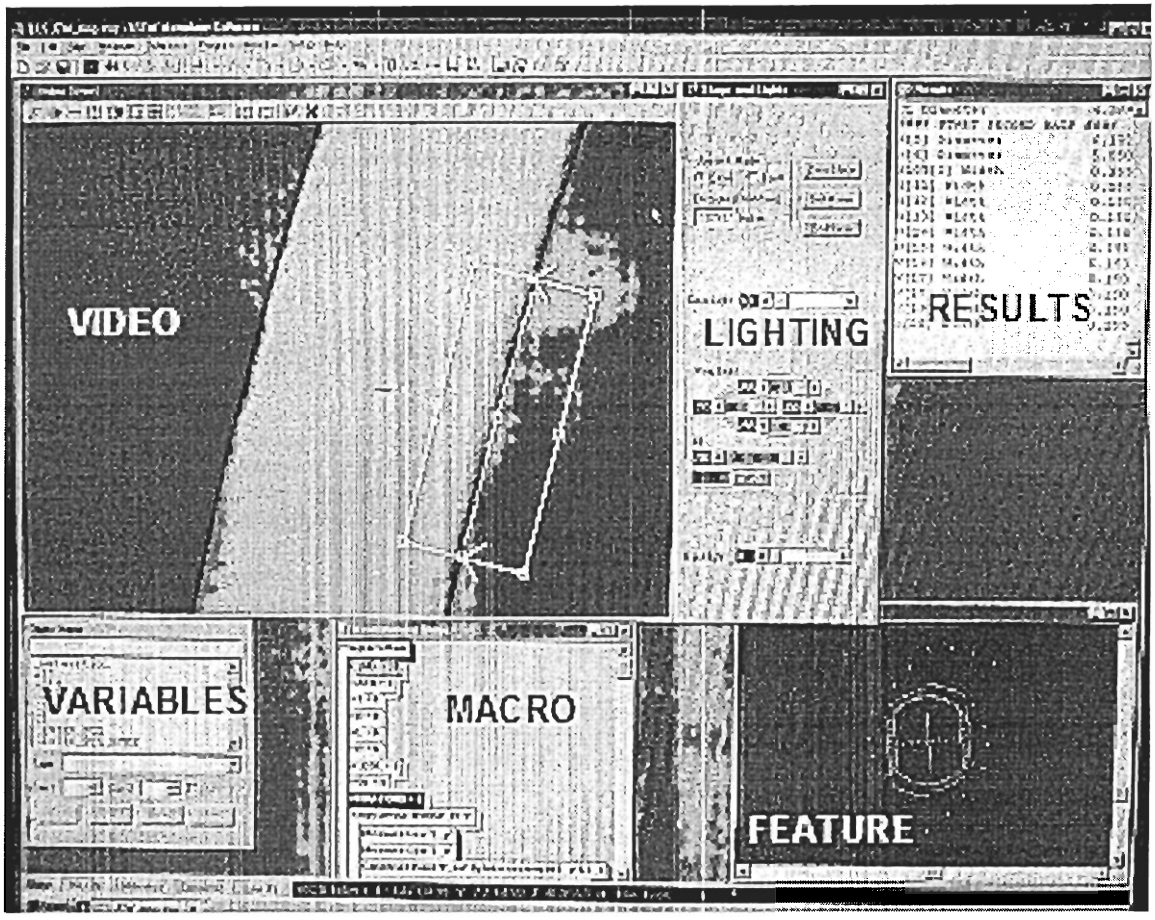

Figure 6.1: Typical scene from VIEW Metrology Software

A macro has been created in VMS to form a template for all current and future inspection programs. The purpose of this macro is to output data to file in two formats: direct measurements taken by the VIEW Metrology Software and XYZ coordinate point clouds of detected edges. These files are generated for each specimen under inspection. The direct measurements consist of all measurements calculated by VMS. Examples of these measurements include points, arcs, circles, lines, slots/linewidths, and distances between entities. The data is saved in ASCII format with user-defined formatting. The coordinate data is also saved in ASCII format, tab delimited in three columns: X, Y, and Z. The XYZ point cloud file contains all of the edge data taken to calculate the direct

measurements by VMS. The point cloud enables the inspection analysis to extend beyond the limits of VMS by using software and methods after the actual measurement.

6.2 QualStar™ 2D V3.0

Extracting the coordinate point cloud from the inspection is extremely valuable to the metrology process for many reasons. It is a record of the edge detection, part orientation, feature location, and completeness of the inspection. The lateral LIGA microstructure geometry usually exceeds the simplicity of basic shapes. Therefore, fitting basic geometry types to the point cloud is not always the most effective solution to obtaining measurements, but an overall contour or "go/no-go" gauging approach is much more desirable. A commercially available software package called QualStar™ 2D v3.0, created by ICAMP, is used to further analyze these point clouds [ICAMP 2003]. QualStar™ enables a linear least squares homogeneous or weighted fit of the data to its respective CAD (*.dxf) design. This package offers scalable vector plotting that clearly shows the deviations of the inspected part to its nominal design. Figure 6.2 is a typical view of the graphical user interface (GUI), of this software package.

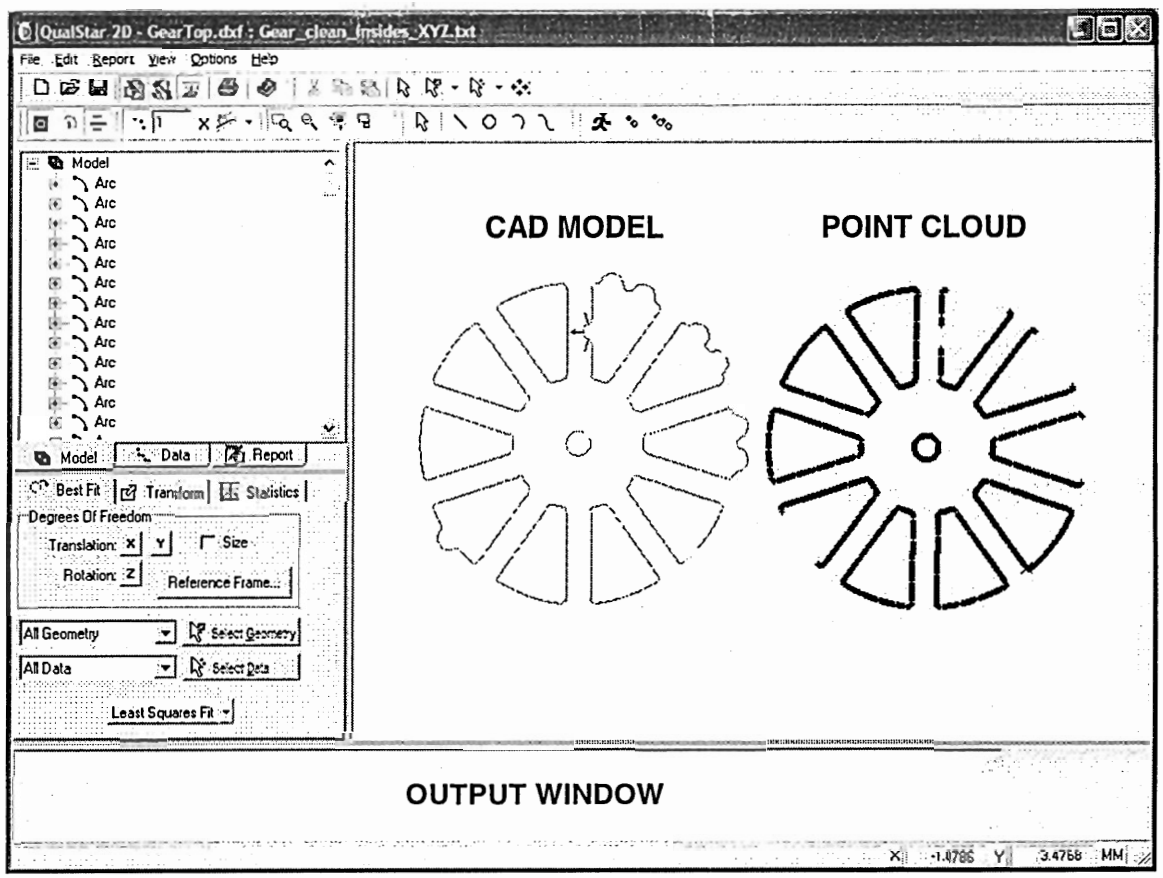

Figure 6.2: QualStar ™ 2D v3.0 user interface

6.2.1 Batch Processing

Reiterating, consistency and statistics are a notable trait of any metrology process, and QualStar™ enables this by its option to create *reports*. The report is a programmable macro that the user may create to run all needed operations on a data set comparison to a CAD model. The report may be saved for future use so that valid comparisons between post-processed data sets can be achieved. Furthermore, QualStar™ has batch processing capability to look at batches of the same part. This requires the user to prepare a text file that contains certain cards for accessing previously created report files, CAD models, and

point cloud data. This option has been used extensively in the LIGA metrology process for part counts on the order of hundreds. When using the batch processing capabilities of QualStar™ on complicated geometries, the point cloud must be aligned, prior to preparing the batch file, to give the fitting algorithm an acceptable initial guess. Once the CAD comparison is complete, the point-to-CAD deviation data, through options specified by the report macro, is saved with respect to the geometry to which it was assigned in the fitting step. The data is exported in single-column ASCII format.

6.3 Matlab™ Software Development

Matlab v6.5 R13 (Version 6.5 Release 13) is the programming environment chosen for creating GUI-based toolboxes for post-processing the direct measurement files and point clouds [Mathworks 2003]. The toolboxes allow the user to view and manipulate point clouds, prepare batch files, perform statistical calculations on large sets of data, and interact with the results. Ultimately, these toolboxes are used to accelerate data reduction and ensure consistency among inspections for dimensional metrology reports and process improvement decisions.

6.3.1 Direct Measurement Toolbox (postVIEW)

In order to batch process and interact with the direct measurements taken by VMS, a GUI-based toolbox was created. The user specifies the location of the folder containing the direct measurement files, and all files within the directory are scanned for features

native to the VMS results file format. File names and their data are loaded into the GUI. Figure 6.3 is a labeled view of the software interface.

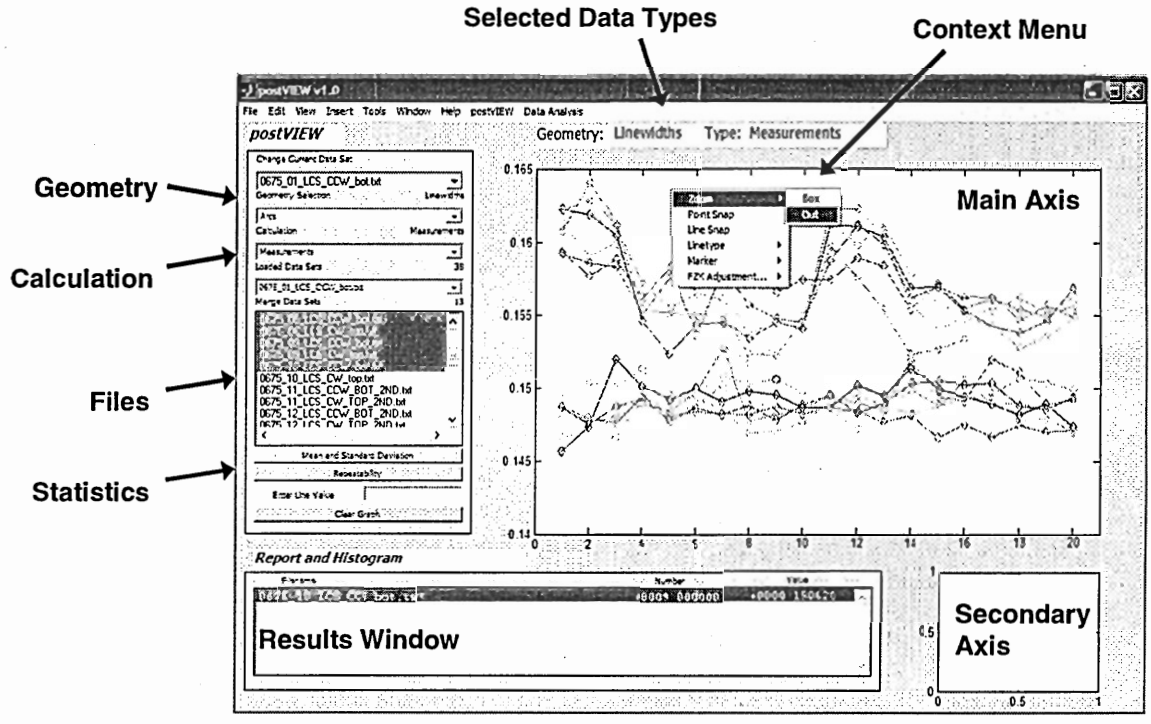

Figure 6.3: Typical scene from direct measurement software

This toolbox allows the user to overlay the data of different parts having similar geometries by selecting file names from the *Files* list box on the left side of the screen. Since some files will contain more than one measurement type, these may be specified from the *Geometry* popup menu. The *Calculations* menu may be toggled between actual measurements or deviations from nominal values for the geometry previously entered in VMS. The selected data types are displayed above the main axis. The secondary axis is used to display a histogram once the mean and standard deviation for each data set are calculated. No legend is present, but the user may query a data point by using the *point*

snap or *line snap* option from the context menu (right-click activation) of the main axis. Once a point is chosen, a red circle is drawn around the point and the information about that point is displayed in the results window. If the *line snap* option is used, a horizontal construction line is drawn through that point so that data points higher and lower may be visualized. A horizontal line may be constructed by entering a value in the *Enter Line Value* edit box.

The statistical capabilities of this toolbox consist of computing the mean and standard deviation of each data set as well as that of all selected data sets. For each data set, the mean value is plotted with bars signifying plus and minus one standard deviation. All statistical results are written to the *Results Window*. The importance of this step is to be able to compare the measurement statistics between files. The user may, for example, choose to compare the statistics of certain measurements across a full wafer or those of a specified part across all process steps. Figure 6.4 shows a typical view once statistics are performed.

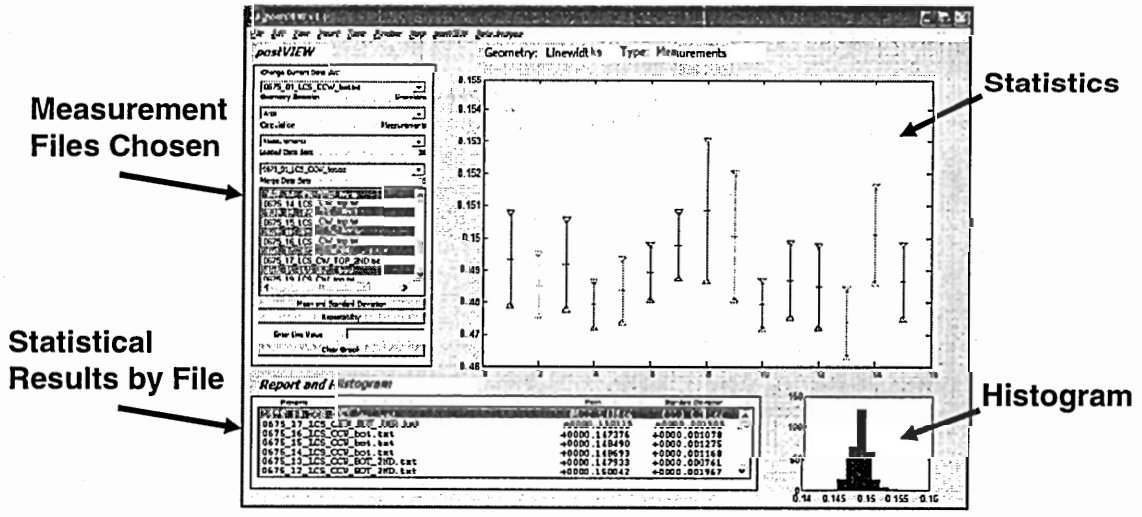

Figure 6.4: Statistics scene from direct measurement software

A large histogram of all accumulated data can be created from the *Data Analysis* menu item. This histogram has adjustable limits and bins sizes. The mean and standard deviation of the accumulated data is printed in the figure.

6.3.2 Point Cloud Viewing and Alignment Toolbox

The coordinate edge data must be aligned prior to batch processing in QualStar™ when complicated shapes are analyzed. A toolbox was created to perform rotation and translation operations on the point cloud so that an acceptable initial guess is given to the fitting routine. Since the fitting routine is two-dimensional, only a two-point model is needed for aligning the points. The model is found by locating a *base point* and an *alignment point* in the CAD file used for the fit. This model may be saved as a *.mod* file and loaded for future use. Figure 6.5 is a labeled screenshot from the alignment software.

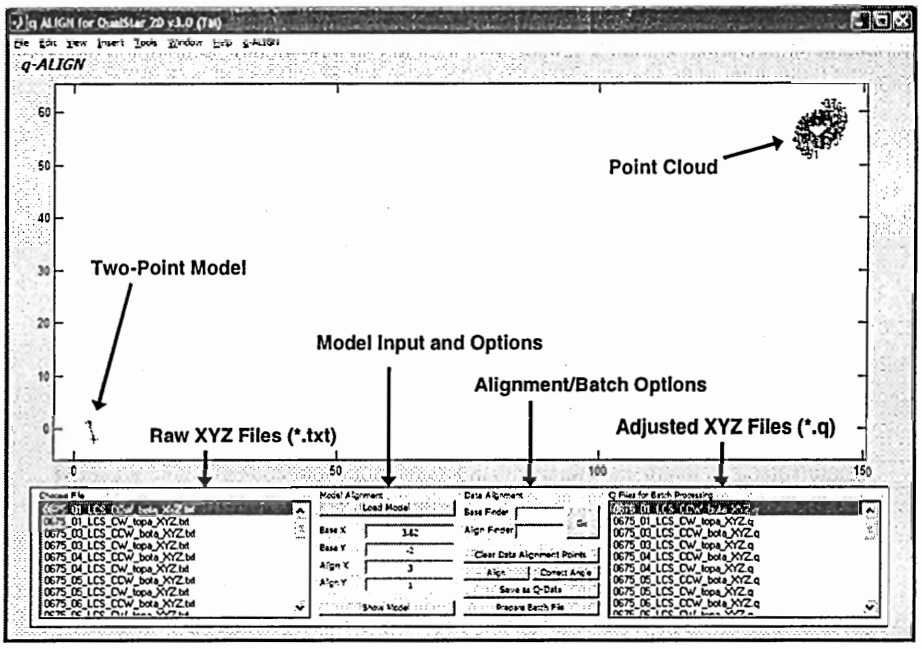

Figure 6.5: Labeled screenshot of alignment software

Once a data set is chosen from the *Choose File* list box, it is displayed in a color-coded plot with labels. The labels are placed to distinguish finders used during the inspection. Aligning the part consists of locating a *base point* and *alignment point* on the point cloud. The data is then manipulated using rotation and translation matrices (Equation 6.1).

$$\begin{bmatrix} x_1' & x_2' & \dots & x_n' \\ y_1 & y_2 & \dots & y_n \\ 1 & 1 & \dots & 1 \end{bmatrix} = \begin{bmatrix} \cos\theta & -\sin\theta & 0 \\ \sin\theta & \cos\theta & 0 \\ 0 & 0 & 1 \end{bmatrix} \begin{bmatrix} 1 & 0 & \Delta x \\ 0 & 1 & \Delta y \\ 0 & 0 & 1 \end{bmatrix} \begin{bmatrix} x_1 & x_2 & \dots & x_n \\ y_1 & y_2 & \dots & y_n \\ 1 & 1 & \dots & 1 \end{bmatrix} \quad (6.1)$$

The translation is defined by the location of the base point on the data with respect to the base point on the model. The angle of rotation θ is defined by the dot product of the

vector formed by the base and alignment points of the model and the base and alignment points of the data (Equation 6.2).

$$\bar{V}_{model} \bullet \bar{V}_{data} = |V_{model}||V_{data}| \cos\theta \tag{6.2}$$

Since the dot product produces only the angle θ and not the direction of rotation, the alignment may rotate the data in the wrong direction. Pressing the *Correct Angle* button resolves this problem.

The adjusted data is saved with a *.q* extension and placed in the *Q Files for Batch Processing* list box on the lower right portion of the screen. These files are now prepared for a QualStar™ batch file. After selecting the desired *.q* files, pressing the *Prepare Batch File* button will prompt the user for a *CAD* file and *Report* file name to add to the selected data files. The batch file, saved with a *.dat* extension, contains all of the needed commands for QualStar™ to execute properly.

This processing step eliminates the need of importing three files (model, data, and report), aligning the data to the model, and adjusting the graphics output settings for each individual data set. When the batch file is prepared, it needs only to be imported after adjusting the graphics output settings in Qualstar ™ once.

6.3.3 QualStar™ Post-Processing Script

Point-to-CAD deviation data are exported from QualStar™ to a one columned ASCII text file. This Matlab script loads the data, sorting each file within the batch as well as the geometry of each file. There are placeholders for file and geometry type, created by output commands of the report file, in the exported deviation file. Two windows are created for each file. The first window contains histograms of the deviation data with respect to geometric entities. The mean and standard deviation of the data are displayed for each data set. The second window has quantile-quantile plots of the corresponding data to the first window. The quantile-quantile plot tests if two data sets come from populations with a common distribution [Weisstein 2003]. In this case, the quantiles of the observed deviation data are plotted against the quantiles of a standard normal distribution. By the nature of this plot, the closer the data fits to a line of slope 1, the closer the data resembles the distribution. Figure 6.6 shows the two windows created for a single data set from a batch process.

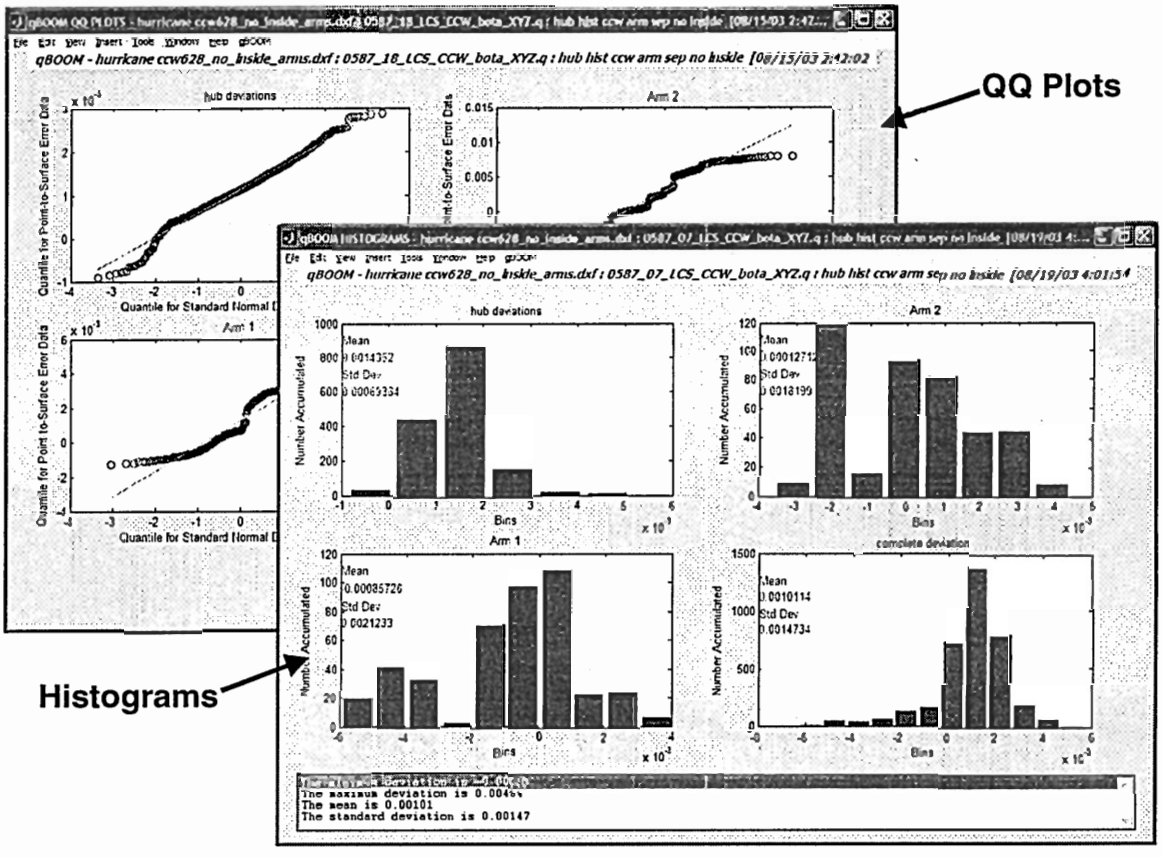

Figure 6.6: GUI Windows from statistics program that processes data exported from QualStar™

6.4 Software Process Flow

By coupling these toolboxes with QualStar™ 2D v3.0, post-processing large amounts of data is a fairly quick task. Figure 6.7 depicts the flow of both types of data, direct measurements and point clouds, from the VIEW Voyager through post-processing and into the final inspection report.

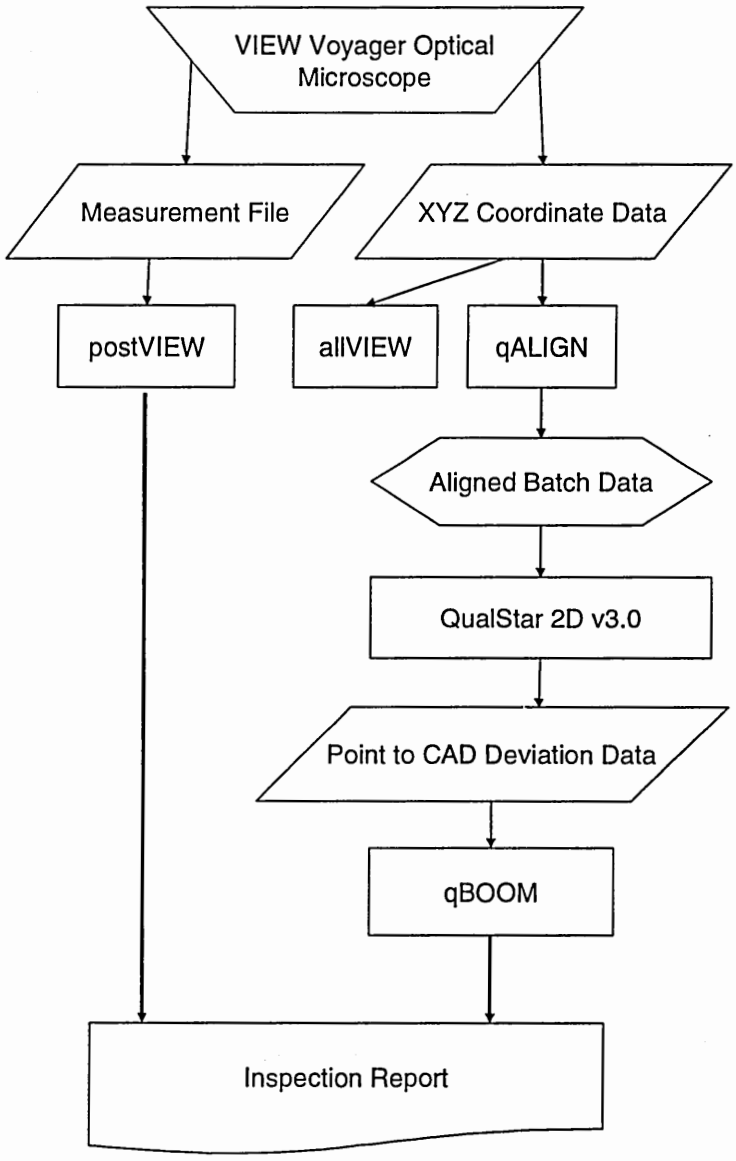

Figure 6.7: Post-processing flow chart

Each package is customized for current requirements and specific parts of the LIGA dimensional metrology effort at Sandia National Laboratories. Graphics, charts, and statistical data are readily available to be included in reports, or exported for further analysis.

CHAPTER 7 : LIGA MEASUREMENT APPLICATIONS

7.1 Customer Dimensional Metrology

LIGA microparts have a wide range of applications. Like semiconductor components, they can be expected to uphold certain thermal and electrical characteristics. Moreover, common micro-mechanical LIGA applications involve designs where structural requirements must be met for features such as flexures and gear teeth. Small variations in geometry can be critical to the fit, performance, and life of the part, so measurements with a statement of inspection uncertainty are necessary.

A LIGA spring design (Figure 7.1), with tolerances on the order of +/-5μm for both feature sizes and contours, was a major factor in developing this metrology process. Most of the research and development of this report was geared towards improving the dimensional inspection of this part design.

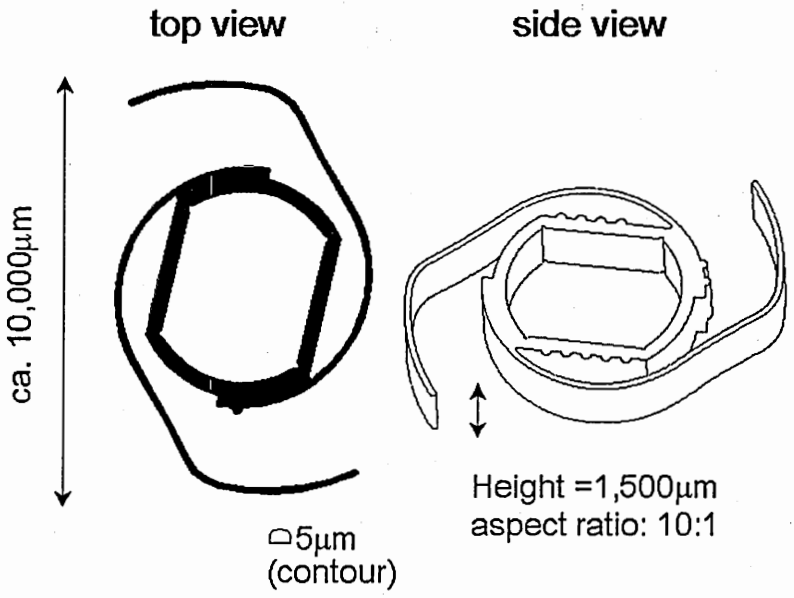

Figure 7.1: A LIGA spring design [Aigeldinger, et al. 2003]

The spring design spans an area of approximately one square centimeter and a thickness of 0.15cm. The arms have a width of 150µm (10:1 aspect ratio) across a arc length of over a centimeter. Other geometric entities under inspection, such as inner arc radii and hub linewidths, have dimensions on a millimeter scale [Aigeldinger, et al. 2003].

The metrology process begins with choosing a microscope objective suitable for the part. The 20x objective has been chosen for this part. The accuracy and reproducibility among different lighting conditions is more favorable with the 20x objective than the 10x objective because of its better resolution for image processing. The critical 150µm linewidth of the two arms of the design fits within the field of view of the 20x objective at any orientation, so the stage uncertainty can be neglected for these direct linewidth measurements. The field of view of the 50x objective is too small to accommodate a

150μm feature. A lighting type and intensity must be defined for the inspection. Due to the understanding gained from the tests performed in Chapter 5, proper lighting for this high aspect ratio metal part would consist of back lighting at high intensity (80%-100%). Next, a VMS macro must be written so that the appropriate edges of the part are inspected consistently over a large batch of hundreds of single parts. This consists of developing a part coordinate system and adding finders in the current VMS template macro. Since the macro is developed, including objective type and lighting environment, the inspection is trivial because variables have been defined to allow to be entered for lighting intensity and edge finding parameters. The inspection program for the LIGA spring design has 105 finders and prompts the user to focus and accept the edge detection at each position. The microscope is equipped with an auto focus option, although it is not used. Experimenting with auto focus options when inspecting LIGA parts has displayed inconsistencies not desirable for the level of inspection required for this part. This enables the user to have total control over how the edge sharpness and inspection quality. Refer to Figure 6.1 for a screenshot of the program inspecting this design. The program inspects ten linewidths per arm, six major arcs, three slots, and takes approximately ten minutes to complete. Desired direct measurements and all points collected from the edge detection are written to file.

Since there are many linewidth measurements, ten per spring arm, in the inspection for this part, the direct measurement toolbox is very useful. All of the arm linewidth measurements are plotted, and the mean and standard deviation are calculated. Figure 7.2 shows a scene from the direct measurement toolbox. Twenty linewidth measurements and

a line representing the average of the data are plotted. The ordinate dimension is in millimeters.

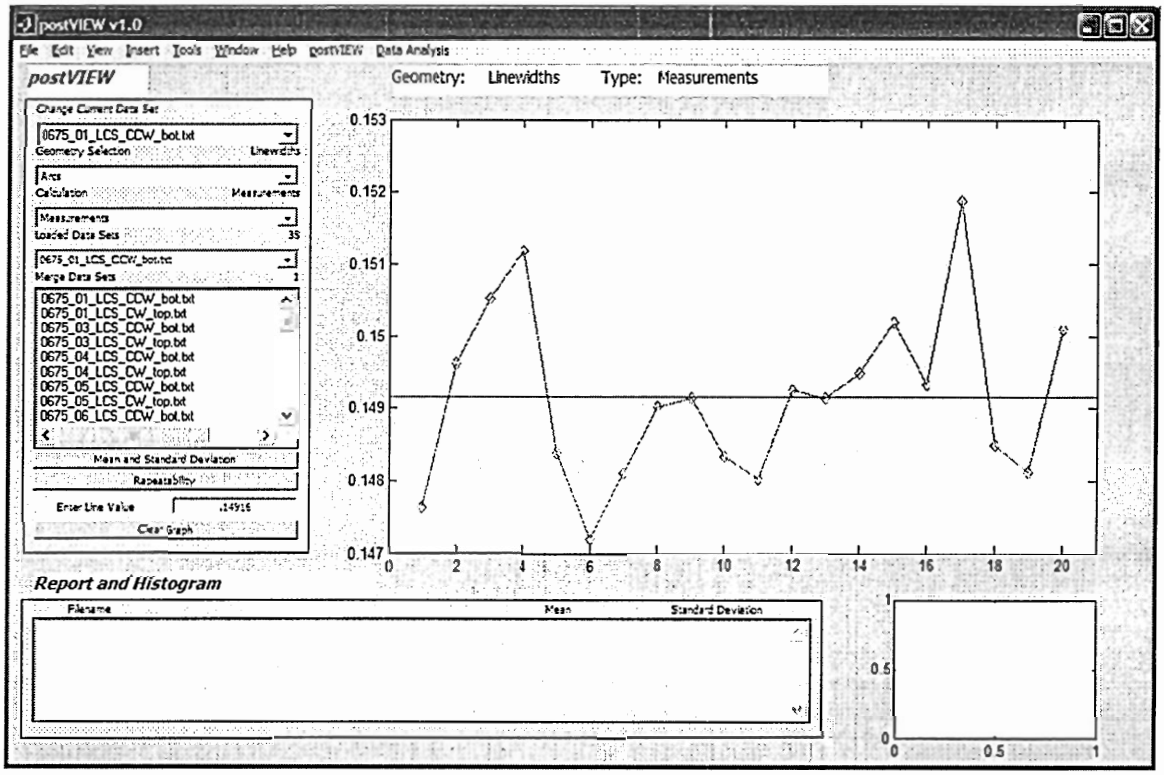

Figure 7.2: Typical scene from direct measurement software

The point cloud data is aligned and then fit to the CAD model for contour inspection. Qualstar™ superimposes a color-coded, scaleable vector plot of the deviation data on the model. Figure 7.3 shows the point cloud and the point-to-CAD deviation plot for this spring specimen scaled to 10x.

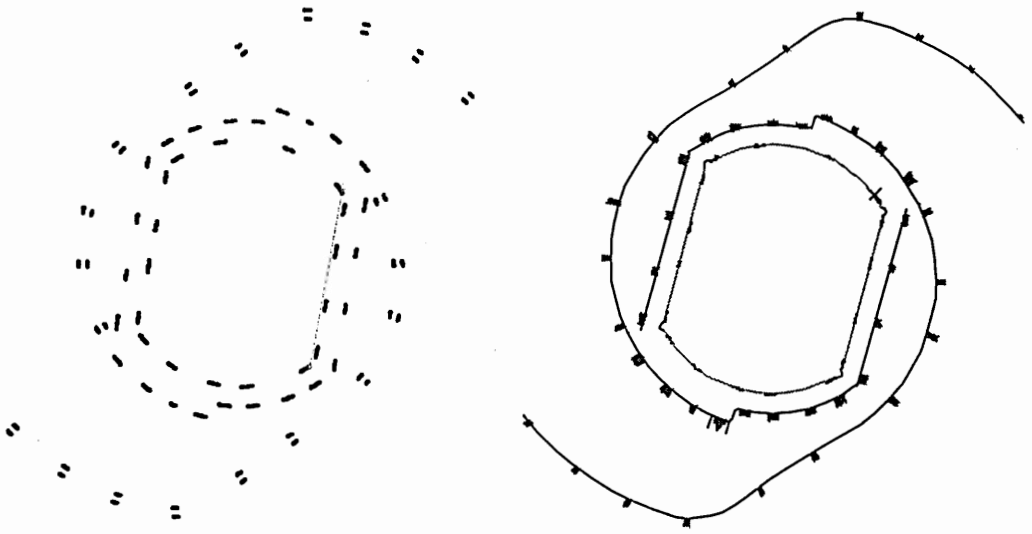

(a) (b)

Figure 7.3: Aligned point cloud (a) and vector plot of deviations (b) on a 10x scale

Along with the vector plot, histograms and QQ plots are created from the deviation data so that the distribution of the data is properly visualized. All of the information and graphics generated from the various toolboxes are placed in the metrology report for each part.

7.2 Metrology for LIGA Process Improvement

The post-processing software scheme has been designed for use in LIGA process improvement. It is not limited to single part dimensional metrology. The processing scripts and GUI-based toolboxes are equipped to handle multiple data sets so that trends from multiple features, parts, wafers, and LIGA process steps may be visualized and analyzed.

LIGA is a manufacturing process with a multitude of copy steps, each step having impact on the next. As data is taken from each step, defects in the process can be observed and improved upon. Data sets may be compared with confidence because of the precautions that have been taken during the inspection and the newfound understanding for the abilities of the microscope to inspect LIGA specimens.

7.2.1 Part Feature Metrology

Mechanical spring performance depends on the effective area of the cross-section of the arms, making these linewidth measurements critical. In the case of the spring design, 150μm thick arms that span over a centimeter in length cannot be inspected sufficiently by taking one measurement; the flexure must be sampled in multiple places. Figure 7.4 shows the inspection points one thorough ten for one of the spring arms.

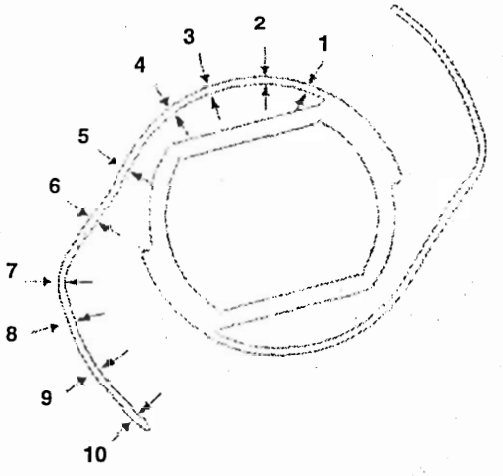

Figure 7.4: Linewidth measurement locations on spring

Linewidths numbered eleven through twenty are taken in the same "armpit to tip" fashion on the opposite arm.

As an example of part feature measurement analysis, the top and bottom surfaces of twenty-four springs from one wafer were analyzed with the direct measurement toolbox. Figure 7.5 shows a plot of the linewidth measurements.

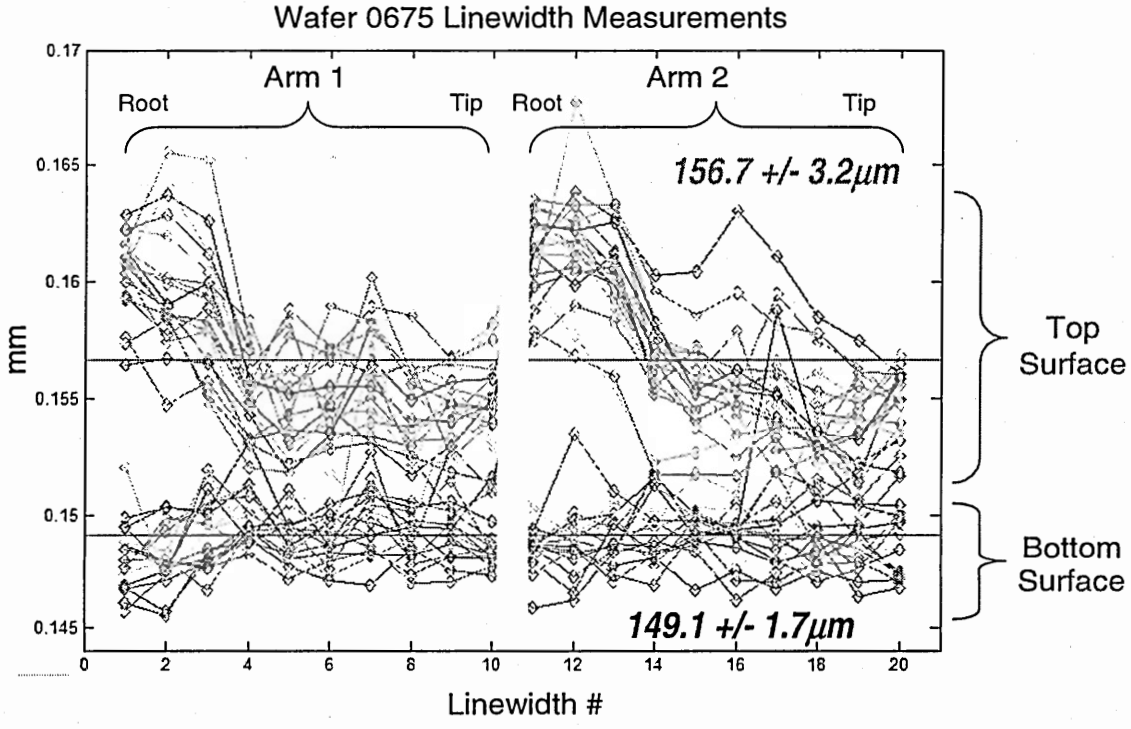

Figure 7.5: Linewidth measurements for top and bottom part surfaces

The linewidths on the top part surface measure 156.7± 6.4μm at 95% confidence. The data shows that the measurement is dependent on arm location. From root to tip, linewidth measurements decrease. This trend has been attributed mainly to the material

properties of the PMMA comprising the mold in which the parts are plated. During the electroplating step, the PMMA mold is submerged in a water-based electroplating bath. The PMMA takes in water, swelling the mold and altering the part sizes [Griffiths and Crowell 2003, Goods, et al. 2003]. The bottom sides of the parts remain unaltered by this effect because the PMMA is bonded to the substrate, inhibiting movement. This effect can also be seen in the QualStar™ fitting analysis when observing the hub portion of the spring. This trend is not present for the bottom surface of the part. The bottom surface linewidths for this wafer measure $149.14 \pm 3.4\mu m$, much closer to the $150\mu m$ design, across the length of the arms. The possible cause of the mean difference between the top and bottom linewidths is from the lapping and polishing process as explained earlier with the stainless steel gauge block.

7.2.2 Part Contour Metrology

Direct measurements such as the linewidth play a large role in understanding the geometry of a part, but their scope is limited. Many times, the contour of the part must also meet a certain tolerance. In a complicated shape, this information cannot be examined through the direct measurements. Hence, point-to-CAD software packages, such as QualStar™, become extremely valuable to inspection schemes. Special care must be taken so that the results from the analysis are meaningful for the function of the part. To analyze the contour of the spring arms, a uniform fit of the data to the model is not necessarily sufficient. The fit must be weighted to the inside hub geometry of the spring so that the position of the arms is measured. The weighting option is built into the

fitting algorithm of the software. This allows the user to flag certain geometric entities and assign a weighting value [ICAMP 2003]. Figure 7.6 shows a non-weighted fit and a weighted fit of the spring.

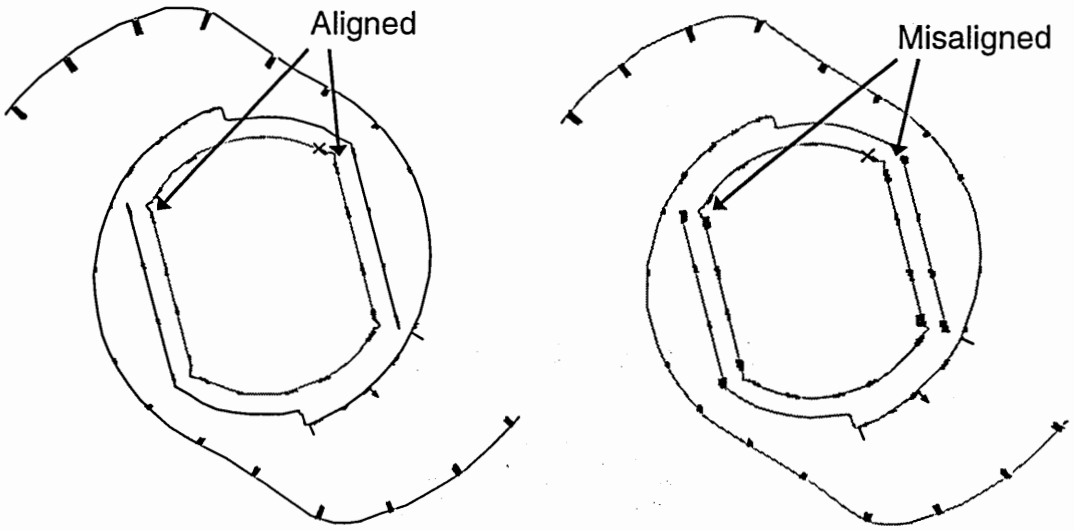

(a) (b)

Figure 7.6: Weighted (a) and non-weighted (b) "best fit" analyses

The above example exhibits an inward displacement of the arms with the increasing deviations from armpit to tip. The arm displacement is noticed on the top and bottom surfaces, and is larger than the effect attributed to PMMA swelling. Processing steps following release from the substrate, such as agitated cleaning and coating may be the cause of the bent spring arms.

The PMMA swelling effect, on the other hand, was examined with contour fits using an accumulation of data from the top and bottom of eleven springs from the same wafer

where arm displacement was not present [Aigeldinger, et al. 2003]. The arm deviation data from QualStar™ was processed. The Gaussian distribution function was fit to both top and bottom data sets. Figure 7.7 shows an overly of the two histograms including the Gaussian fits.

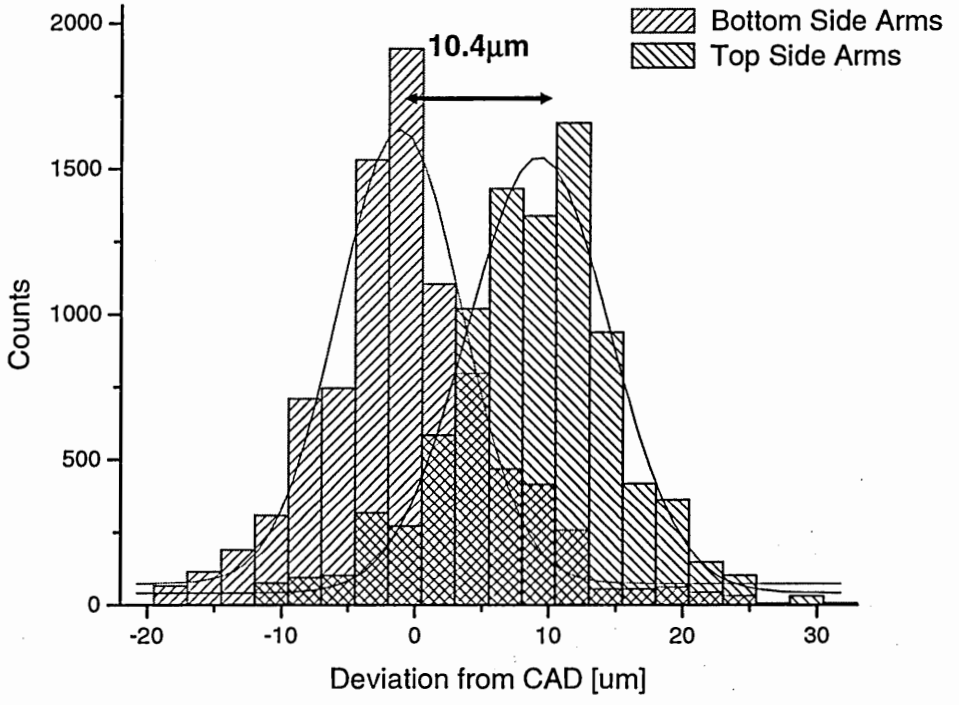

Figure 7.7: Histograms of top and bottom surface deviation data [Aigeldinger, et al. 2003]

The peaks of the fit functions show a 10.4μm difference between the top and bottom outer contours of the springs. Thus, the post-processing scheme is able to quantify the PMMA swelling effect on the spring arms. These results correlate to those predicted by finite element simulations. The finite element simulation produced an 8.2μm change compared to the observed 10.4μm [Griffiths and Crowell 2003]. This swelling study was

made possible by the ability of the post-processing software to sort and accumulate data from multiple QualStar™ deviation files with speed and limited effort.

7.2.3 Whole Wafer Metrology

The LIGA process at Sandia National Laboratories typically uses a three-inch diameter circle for the design boundary. A polar array containing eight springs on the inside diameter and sixteen springs on the outside was a layout for the spring production. All springs on a PMMA mold, stemming from an experiment used to evaluate a synchrotron, were inspected and a plot of the point clouds is shown in Figure 7.8.

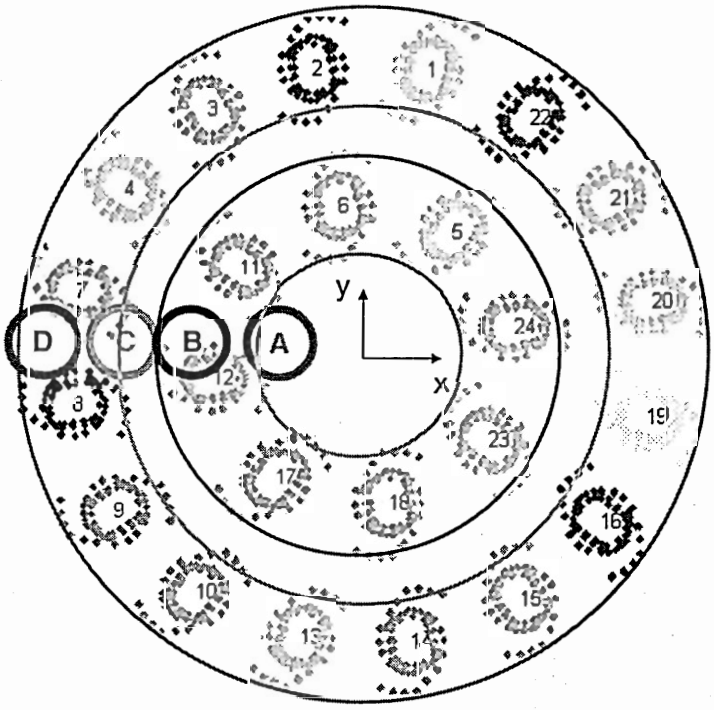

Figure 7.8: Point cloud of full wafer inspection

The linewidths of this wafer's springs in PMMA were plotted using the direct measurement software, and the same trend was present with respect to the "root to tip" positioning of the measurement, indicating the swelling effect of the PMMA. However, another trend was noticed once the linewidths from the eight springs located on the inside diameter and the outer sixteen springs were plotted separately. Figure 7.9 shows both linewidth plots.

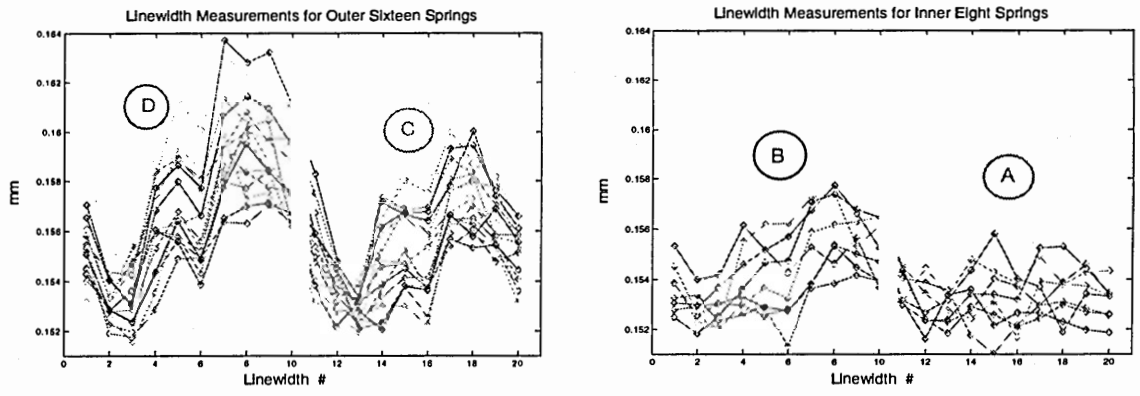

(a) (b)

Figure 7.9: Linewidth plots of outer (a) and inner (b) springs with respect to wafer position

A trend is present that shows that the linewidth size is dependent on its location on the wafer. The average linewidth measurement decreases by three microns on average from the outer to the inner position. Refer to Figure 7.8 and Figure 7.9 to match the plotted values to the wafer positions (A-D). An effect like this may be attributed to a defect in the gold mask, inhomogeneous water uptake/swelling of the PMMA, or the makeup of the synchrotron exposure tool that exposed the PMMA. To understand the

cause of this effect, the mask used to create the mold was inspected, and both data sets were plotted together (Figure 7.10).

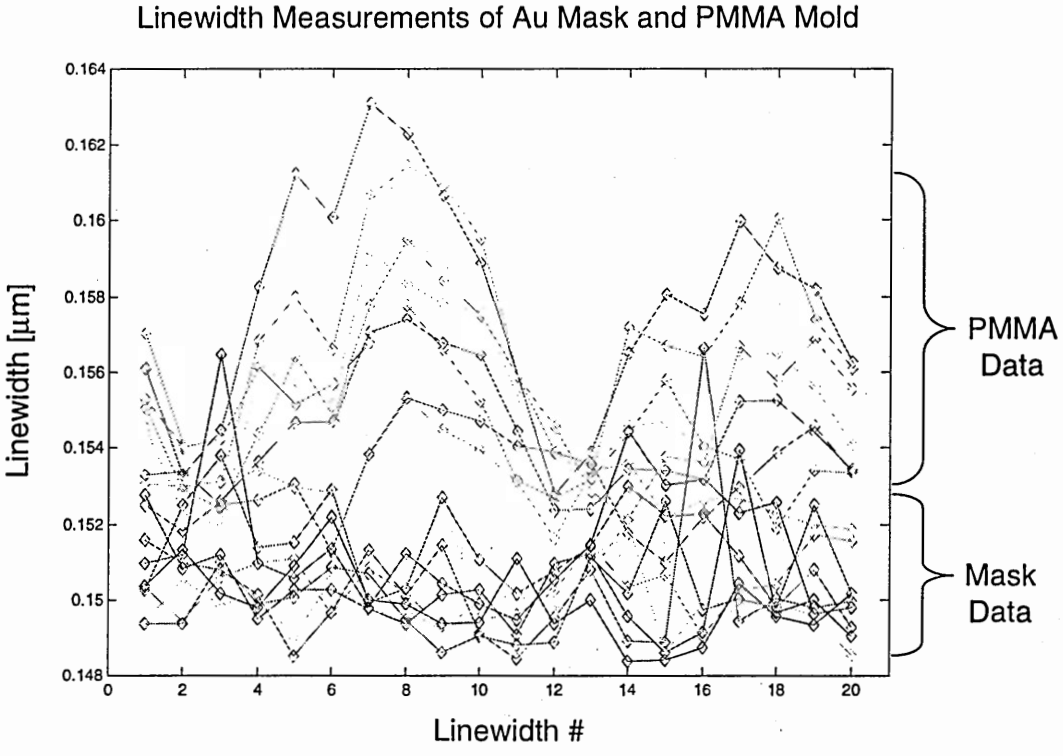

Figure 7.10: Comparison plot of mask and PMMA linewidth data

The comparison graph shows that there is no evidence that the trends seen in the PMMA are due to mask defects. The difference between the two steps can most likely be attributed to the swelling effects of the mold. Although overlaying the data does not instantaneously pinpoint the source of the error, it does allow for certain theories regarding process defects to be nullified; such as a mask defect in this case.

7.2.4 Metrology Across Process Steps

Dimensional metrology data should be taken at all steps since every step of the LIGA process has an effect on the final part. When a defect is present in a final part, it is extremely beneficial to be able to trace the problem to the step where it occurred. It is also beneficial to abort the process when a mask or mold does not meet specifications. The direct measurement analysis software was created with this in mind. Therefore, data from the chrome mask, gold mask, PMMA mold, and released parts (top and bottom) can be plotted simultaneously to observe the variation of the geometries throughout the LIGA process. Figure 7.9 uses the direct measurement analysis software to plot the linewidths of the same spring from process start to finish.

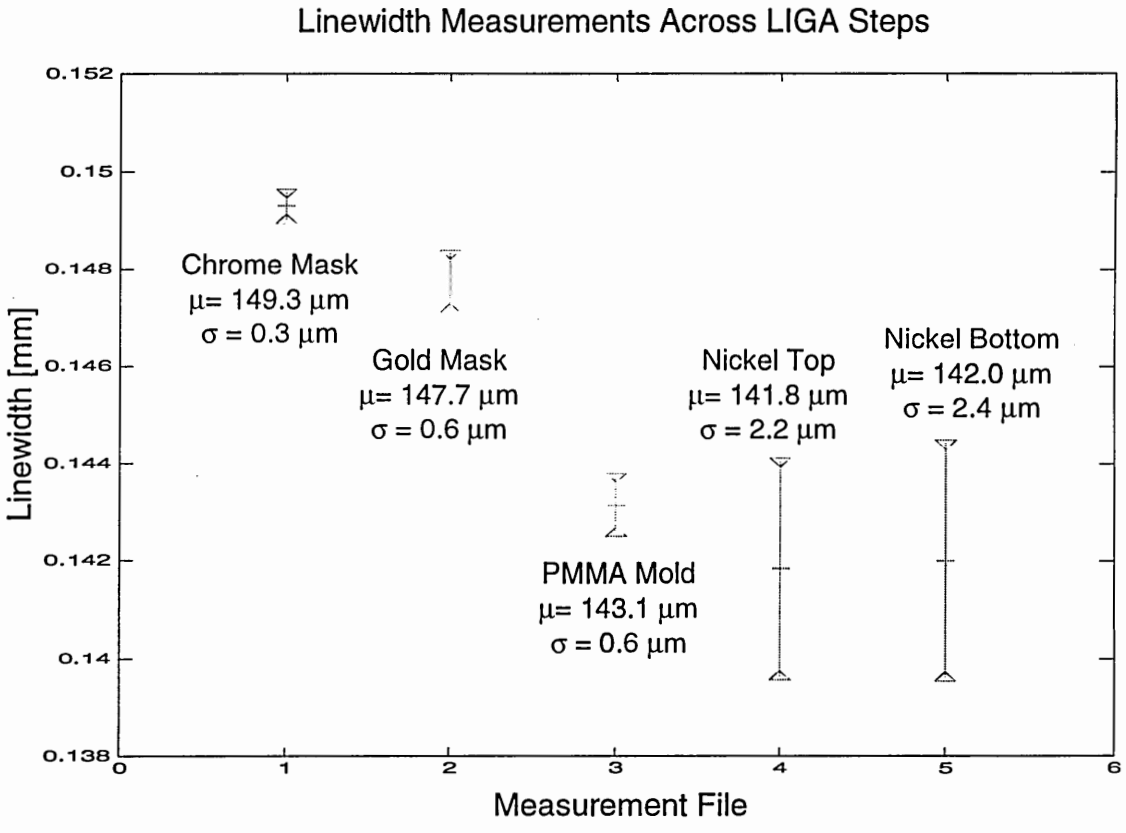

Figure 7.11: Metrology across all LIGA process steps [Aigeldinger, et al. 2003]

The above graph contains an abundance of information that must be carefully understood before conclusions are made. Each measurement file contains twenty linewidth measurements; mean and standard deviation bars are plotted above for one spring. The chrome mask was patterned to produce a 150μm linewidth. The standard deviation for the chrome is and should be the smallest across process steps because it is the first and most accurate step of the process, producing a high-contrast, sharp edge during inspection. The gold mask was inspected at the top surface of the SU8 photoresist structures. If the SU8 sidewalls exhibit any skew, the measurement will be smaller because the gold absorber will be wider. The PMMA was inspected under the same

lighting environment as the SU8 prior to electroplating. The transition between these two steps has the largest difference across mean values (4.6μm). Moving from the PMMA to the released parts, the mean linewidth decreases and the standard deviation increases. During plating, the mold is immersed in a water-based bath for a long period of time. Consequently, the PMMA becomes saturated, and the swelling effect is at a maximum when the parts are formed. The mold was not fully saturated during its inspection, since the mold was not yet submerged in the electroplating bath. Hence, the two micron difference is explained. Regarding the released parts, Nickel Top and Nickel Bottom, the standard deviation is much larger than that of the previous steps. This may be attributed to lapping and polishing procedures, edge roughness, corrosive attack on the material from the release chemistry, or swelling effects at maximum water uptake. Ultimately, with an understanding of the fundamentals of each process step, much can be learned and quantified from overlaying data across process steps.

CHAPTER 8 : CONCLUSIONS

The microscope was examined to understand its measurement capabilities along the lines of lighting environment, repeatability, and accuracy for LIGA high aspect ratio structures and process steps. The studies present the obstacles that may be encountered with LIGA inspection and explain how to control them. Methods of assessing uncertainty to the inspection are also addressed for absolute measurements and comparisons of measurements across lighting environments.

Metrology software was developed to couple commercially available software to automate and accelerate the post-processing effort once data is acquired. The purpose for developing these dimensional metrology toolboxes was two-fold: for customer metrology reports and for process improvement through data analysis. Although this post-processing effort has been implemented for LIGA specimens, it may be applied to other manufacturing processes.

8.1 Limitations

The inspection of LIGA process steps has its limitations. Primarily, the accuracy of the system is limited to the certification accuracy of the calibration standard. As shown in chapter four, this microscope has demonstrated the ability to measure with less uncertainty than the certified standard currently used. The same concept applies to the stage. The uncertainty found is dependent on the certification accuracy of the calibration grid plate.

As features become smaller, the obvious choice would be to use a higher magnification lens. Focusing now becomes a challenge because the depth of focus of the lens is on the submicron scale, in the case of the 50x objective presented in this study. Due to the scale of parts tested in this study and their edge topology, it is recommended that the 10x and 20x objectives are used to easily obtain focus. As features become smaller, the 50x objective will be desired, but inspection quality will be hindered unless edge topology can be refined to improve sharpness and contrast for image processing.

In the case of gold mask inspection, only the top surface of either the SU8 or Novolac can be inspected. The accuracy of this data is dependent upon the normality of the photoresist sidewalls. If a retrograde (Figure 8.1) is present in the resist structure, for example, the measurement results will be larger for the linewidths that are exposed.

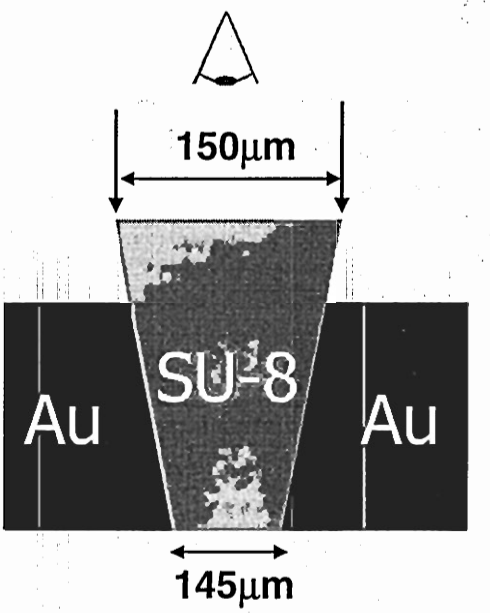

Figure 8.1: SU8 exaggerated retrograde

The arrows indicate where the optical microscope will detect edges, but the outer edge of the gold absorber will prohibit X-ray penetration into the PMMA, resulting in a smaller linewidth on the PMMA mold. This applies for released structures, also. However, more information may be obtained because the bottom surface can be inspected as well. The sidewall cross-section can be roughly estimated, but the true sidewall profile must be acquired through the use of other tools.

The amount of data acquired during inspection is dependent on the number of finders used in the inspection program. An increase in the number of finders will increase the data acquisition time as well as the size of the data sets. Large data sets may become time consuming for batch processing. Therefore, as part production increases, inspection times must be able to maintain process flow, requiring an efficient, yet effective inspection scheme.

8.2 Recommendations

As defined in the limitations section, the more accurate the calibration standard, the more accurate the inspection. Thus, higher resolution standards are recommended to further decrease the uncertainty of the measurement in the optics and stage of the microscope.

LIGA part inspection does not require the full inspection area of the stage, so a standard should be acquired to determine the uncertainty involved with wafer- and part-sized areas. These reticles will produce hard data that has the potential to lessen the uncertainty of the stage depending on the area spanned during each inspection scenario.

Maintaining the calibration of the instrument is also important. Frequent diagnostics such as stage and optics calibration are performed and documented to assess machine performance and possible depreciation.

LIGA metrology is a developing science. A constant effort to improve data acquisition capabilities and data processing techniques is necessary to advance this technology. The purpose of this research is to serve as a foundation for dimensional metrology efforts aimed toward understanding and advancing the state of the art of LIGA microfabrication.

REFERENCES

Aigeldinger, G., J. Ceremuga, J., and D. M. Skala, (2003). "Large Batch Dimensional Metrology Demonstrated in an Example of a LIGA Fabricated Spring," *Sandia Report*, Sandia National Laboratories, Livermore, CA.

Brighton Webs Ltd., (2003). http://www.brighton-webs.co.uk/Statistics/default.asp.

Choi, W. (1996). "Computational Analysis of Three Dimensional Data," Carnegie Mellon University, Pittsburgh.

Davis, McNabb, et al. (2001). "General Workmanship Requirement 9900000," Albuquerque, NM.

DOW Chemical (2003). "Products for UV/Photocure Coatings," http://www.dow.com/epoxy/products/a-coatings/photocure.htm.

Dow, T. A. and R. O. Scattergood (2003). "Mesoscale and Microscale Manufacturing Processes: Challenges for Materials, Fabrication, and Metrology," *ASPE 2003 Winter Topical Meeting*, ASPE, University of Florida.

Goldstein, J. I., D. E. Newbury, et al. (1992). "Scanning Electron Microscopy and X-Ray Microanalysis," Plenum Press, New York.

Goods, S., Howard, S., et al. (2003). "Thermal Expansion and Hydrogen Behavior of PMMA Molding Materials for LIGA Applications," *Sandia Report*, Sandia National Laboratories, Livermore, CA.

Griffiths, S. K. and J. A. Crowell (2003). "Dimensional Errors in LIGA-Produced Metal Parts due to Thermal Expansion and Swelling of PMMA," *HARMST 2003*, Monterey, CA.

Harris, E. F. (1969). Dimensional Metrology, The General Electric Company, Dearborn.

Hecht, E. (2002). Optics, Addison Wesley, San Francisco.

Hibbard, R. L. and M. J. Bono (2003). "Meso-Scale Metrology Tools: A Survey of Relevant Tools and a Discussion of Their Strengths and Weaknesses," *ASPE 2003 Winter Topical Meeting*, ASPE, University of Florida.

Hoskins, M. E. (1969). Taking a SWIPE at Metrology. Battelle Memorial Institute, Dearborn.

ICAMP (2003). *QualStar™ 2D v3.0*, http://www.icamp.com.

I.C.E. (1998). Practical Integrated Circuit Fabrication Seminar. Integrated Circuit Engineering Corporation, Scottsdale, AZ.

IMM (2003). "LIGA Technology," Institute fur Mikrotechnik Mainz.

JEOL (2003). "A Guide to Scanning Microscope Observation," JEOL USA.

Madou, M. (1997). Fundamentals of Microfabrication, CRC Press, Boca Raton.

Mathworks (2003) *Matlab Version 6 Release 13*, http://www.mathworks.com.

Menz, W., J. Mohr, et al. (2001). Microsystem Technology, 1st Edition, John Wiley and Sons.

NIST (2003). "Physical Reference Data," http://physics.nist.gov/cuu/, National Institute of Standards and Technology.

NIST (1994). "Guidelines for Evaluating and Expressing the Uncertainty of NIST Measurement Results," *NIST Technical Note 1297,* Gaithersburg, MD.

Olszak, A. G., J. Schmit, et al. (2001). Interferometry: Technology and Applications, Veeco Metrology Group: 4.

Vezzetti, C. F., R. N. Varner, et al. (1991). "Bright-Chromium Linewidth Standard, SRM 476, for Calibration of Optical Microscope Linewidth Measuring Systems," *National Institute of Standards and Technology,* Gaithersburg, MD.

VIEW Engineering (2003). http://www.vieweng.com.

Waldo, W. (2001). "Techniques and Tools for Optical Lithography." Handbook of VSI Microlithography 2001 2nd Edition: 552-555.

Weisstein, E. (2003). "Quantile-Quantile Plot," *Wolfram Research*, http://mathworld.wolfram.com/Quantile-QuantilePlot.html.